

Planetary growth in turbulent discs before the onset of gravitational instability

A. Hubbard^{1,2}, E.G. Blackman^{1,2}

1. Dept. of Physics and Astronomy, Univ. of Rochester, Rochester, NY 14627; 2. Laboratory for Laser Energetics Univ. of Rochester, Rochester NY, 14623

ABSTRACT

Standard models for planet formation require gravitationally unstable discs. Initially unstable gas-dust discs may form planets directly, but the high surface density required has motivated the alternative that gravitational instability occurs in a dust sub-layer only after grains have grown large enough by electrostatic sticking. Although such growth up to the instability stage is efficient for laminar discs, concern has mounted as to whether realistic disc turbulence catastrophically increases the settling time, thereby requiring additional processes to facilitate planet formation on the needed time scales. To evaluate this concern, we develop a model for grain growth that accounts for the influence of turbulence on the collisional velocity of grains and on the scale height of the dust layer. The relative effect on these quantities depends on the grain size. The model produces a disc-radius dependent time scale to reach the gravitationally unstable phase of planet formation. For a range of dust sticking and disc parameters, we find that for viscosity parameters $\sim 10^{-3}$, this time scale is short enough over a significant range in radii R that turbulence does not catastrophically slow the early phases of planet formation, even in the absence of agglomeration enhancement agents like vortices.

Subject headings: accretion discs – planetary systems: formation – planetary systems: protoplanetary discs

(Submitted to MNRAS)

1. Introduction

Planets are believed to form in the gas and dust discs that surround newly formed stars. In principle, planets can form purely from gravity, via direct gravitational instability

in the initial circum stellar disc (Boss 1997). However, this mechanism of planet formation requires higher initial densities than commonly presumed. For a standard MM SN (minimum mass solar nebula) model for the gas and dust discs around a young star, both the initial dust and gas discs are gravitationally stable and the only force available for the early protoplanetary stage of planet formation is electrostatic sticking. For planets to form, the dust must therefore grow from electrostatic forces until gravity can play a significant role.

The basic model for how such a state could arise was put forth by Goldreich and Ward (Goldreich & Ward 1973), hereafter GW. In their proposed route to planet formation, dust grains initially collide and stick. The growing grain mass eventually reduces the dust's thermal velocity dispersion and therefore, the scale height of the dust disc. Eventually the grains settle into the disc's mid-plane until the critical density at which this dust disc becomes gravitationally unstable is reached and the formation of kilometer sized planetesimals is facilitated. Subsequent accretion of surrounding gas would then complete the core-accretion model for giant planet formation. Recent observations of CoKu Tau/4 (D'lessio et al. 2005) seem to imply that massive planets must be able to form within 10^6 yr, which is the tightest constraint to date on the total available time for any planet formation mechanism.

In the absence of turbulence in the gas disc, the GW model is very efficient and the time scale to grow grains to the size at which enough settling occurs for gravitational instability to occur is a small fraction of 10^6 years. However, Weidenschilling (Weidenschilling 1980) argued that turbulence can catastrophically prevent the required early growth phase by stirring up the dust disc, thereby delaying or preventing the subsequent gravitational instability. Because of prevalent sources of disc turbulence (such as dust-gas shear, Cuzzi et al. (1993), Charnley et al. (1995) and MRI instability Balbus & Hawley (1991)) a turbulent disc is likely the norm rather than the exception and the GW theory must be revisited. Ironically, even turbulence driven from the dust settling itself (Ishitsu & Sekiya 2003), might prematurely quench the GW process.

The potential show-stopping effect of turbulence has led to a substantial body of work incorporating additional physics, such as anti-cyclonic vortices, that can accelerate the agglomeration of dust grains should the early GW phase fail. But even if extra processes are present and helpful, the need for such processes has remained unclear. Despite the conceptual concerns induced by turbulence, its actual effect on planet growth has not been conclusively calculated. Regardless of the details of the turbulence, there will exist a dust grain size for which the effects of the turbulence are sufficiently weak that the GW process can proceed to instability. The question therefore is whether the presence of turbulence catastrophically slows grain growth before that size can be reached. We attempt to answer that question.

The effect of turbulence on dust growth is two-fold. On the one hand it can increase the

dust's collisional velocities (and so the collisional rate) which is a positive effect for growth. Some early work on this was done by Voelk et al. (1980). On the other hand, it increases the scale height of the dust which acts to decrease the density (and so the collisional rate) and to prevent instability. Understanding the net effect of turbulence amounts to understanding its relative effect on these two velocities as a function of grain size and radial location. In this paper we develop a model for the time evolution of grain growth as a function of dust size and disc location to determine how long it takes for the grains to grow large enough to settle in the disc and reach the gravitationally unstable density. We do not discuss the physics of the post-gravitationally unstable regime.

In section 2 we derive the basic equation for grain growth and describe the disc model and how turbulence and drag on grain motion is included. The grain growth equation depends on the ratio of dust collisional velocity and the velocity determining the dust scale height. In section 3 we derive explicit formulae for these key velocities. In section 4 we show that there are 6 regimes for the combination of these velocities and discuss how grain growth proceeds as a progression through these regimes. In section 5 we collect key results for the final grain sizes and time scales needed to get to the scales at which the disc becomes gravitationally unstable for fully turbulent discs and for discs with dead zones. In section 6 we discuss the implications of our results for constraining the strength of turbulence for which rapid planet growth can still occur. We conclude in section 7.

2. Basic model of dust grain growth in a turbulent disc

We consider a protoplanetary disc to be a dust disc embedded in a turbulent gas disc. At any one time, we approximate all dust grains as spherical with identical radii r_d , constant density ρ_d and hence dust-dust collisional cross-section $\sigma_{dd} = 4 \pi r_d^2$ and mass $m_d = \frac{4}{3} \pi r_d^3 \rho_d$. Although the dust in a real disc would have a spectrum of sizes, without a detailed sticking and destruction model for collisions the, extra complication involved with using a spectrum does not guarantee extra precision for the present calculation. To encapsulate the unknown physics of dust-dust interactions, we presume that a collision between two dust grains has a probability c to result in sticking. If such a collision does not result in sticking the grains are presumed to be unchanged. Accordingly we can see that, if \dot{N} is the dust-dust collision rate then $\frac{dN_d}{dt} = c \dot{N} m_d$ and so using the equation for $m_d(r_d)$,

$$\frac{dr_d}{dt} = \frac{c}{3} \dot{N} r_d: \quad (1)$$

As dust grain size is a key parameter, which we investigate the change of as a function of the distance from the star we will presume that dust grains do not significantly migrate radially.

2.1. Equation of grain growth

If we use a simple "particle-in-a-box" collision model we find that

$$N = \frac{1}{m_d} \frac{dV_c}{dV_h} = \frac{d}{H_d m_d} \frac{dV_c}{dV_h} = \frac{d}{m_d V_h} \frac{dV_c}{dV_h} = \frac{3}{d r_d} \frac{V_c}{V_h}; \quad (2)$$

where H_d is the dust disc scale height, m_d and r_d are the dust disc volume and surface densities, Ω is the orbital angular velocity, v_c is the dust-dust collisional velocity, and v_h is the effective velocity dispersion relative to the Keplerian disc used to determine $H_d = \frac{v_h}{\Omega}$. The dust and gas scale heights need not be equal, the latter being given by $H_g = c_s^{-1}$, where c_s is the gas thermal speed.

If $v_c = v_h$ in (2), then $N \propto r_d^{-1}$. It follows that if $\Omega = 1 \text{ cm}^{-3} \text{ s}^{-1}$, $\frac{dr_d}{dt} = 107 \frac{\text{cm}^3}{\text{AU}^2 \text{ yr}^{-1}}$ is independent of dust size and the formation of meter sized bodies will occur in 1 year. As without turbulence, gravitational instability of the disc will occur for sub-centimetre sized grains (60); this process occurs well within the time scales required by existing constraints (e.g. D'Alessio et al. (2005)) even considering settling times. If, however we introduce turbulence into the gas disc there is no reason to presume that $v_c = v_h$ or that the two are cleanly related. While it is difficult to imagine v_c being greater than v_h , the reverse is plausible, for example when the dust grain velocities are strongly correlated. If the dust couples strongly to the gas and the turbulence causes significant mass mixing throughout the gas disc, then v_h can be approximated by c_s , the gas sound speed. In addition, very small grains will have the same bulk velocity as any turbulent eddy in which they reside, and will interact with collision velocities corresponding to the dust thermal speed, i.e. $v_c = v_{th}$. Even for small dust grains, $c_s > v_{th}$ so the dust growth rate would be prohibitively low if such $v_c < v_h$ held for large ranges of r_d .

We can, however, imagine that as the dust grains grow and couple less strongly with the gas, the turbulence can collide dust grains with collisional speeds $v_c - v_{turbulent} > v_{th}$. Eventually the growing dust grains will settle out of the gas disc, so that v_h will decrease. For very large dust grains, with mean free paths (with respect to each other) longer than the largest scale eddies, the ratio v_c/v_h approaches 1, drastically increasing the growth rate (3) above the value for very small grains.

To facilitate deriving the regimes of v_c and v_h in detail, we define $\alpha = \frac{d}{dr_d}$, which is proportional to a single dust grain's surface density. Then, presuming a constant Ω , we can combine (1) and (2) to obtain:

$$\frac{d}{dt} = \alpha \frac{v_c}{v_h} \quad (3)$$

The variable α will later help clarify the effects of different dust grain densities on time scales and critical grain sizes. As $\frac{d}{v_h}$ is the dust density in the disc, $\alpha = \frac{v_c}{v_h}$ is the surface density

of the dust sheet that a dust grain travels through in time dt . Hence (3) states that the sticking parameter modified surface density of that sheet can be added to the penetrating dust grain's surface density, much like throwing a ball through cling wrap.

The basic question we seek to answer is whether the grain growth is sufficiently rapid that the gravitationally unstable regime for planet formation can be reached long before the total time scale available for planet formation ($\sim 10^6$ yr, D'Adda et al. (2005)). In our pursuit, we need to consider that very rapid collisional velocities could be too high for sticking to occur and instead result in the destruction of the grains. We also need to determine how large the grains must become for them to settle out and allow gravitational instabilities to occur. While there exists a dust scale above which the effect of turbulence on the dust velocity dispersion decreases sufficiently for the dust disc to be gravitationally unstable, that size scale will be far greater than the initial size of the dust as well that the critical size in the absence of turbulence.

To address these issues, we determine the various regimes for v_c and v_h before the onset of gravitational instability. These regimes depend on the quantities r_d , c_s , the turbulent viscosity parameter and the mean free path of the gas l_{mfp} . We then use (3) and the values for the ratio of v_c and v_h to calculate the peak collisional velocities and the total growth time before the onset of gravitational instability.

2.2. Disc model

We assume the disc has an essentially isotropic turbulent viscosity

$$\tau' \propto M^{-1/2} H_g; \quad (4)$$

where v_M and M are the maximum turbulent velocity and length scales in our assumed Kolmogorov spectrum and τ is the Shakura-Sunyaev viscosity parameter (Shakura & Sunyaev 1973). Using $M = v_M$, $1 = H_g = c_s$, and (4) it follows that

$$M^{-1/2} \propto \tau^{1/2} H_g \quad (5)$$

$$v_M \propto \tau^{1/2} c_s; \quad (6)$$

If τ is extremely low, the GW process will proceed as accordingly as in the absence of turbulence. It is likely that at least dust-gas shear (e.g. Ishitsu & Sekiya (2003)) prevents τ from dropping to values where it could otherwise be ignored. Our model will involve a progression of dust growth regimes whose order requires approximately $2 \times 10^{-6} < \tau$. If τ falls below that lower bound then our regime ordering would need to be modified.

We take a minimum mass solar nebula (MM SN) model with the following scalings from Sano et al. (2000):

$$g(R) = g_0 \frac{R}{1\text{AU}}^{\frac{3}{2}} \quad (7)$$

$$T(R) = T_0 \frac{R}{1\text{AU}}^{\frac{1}{2}} \quad (8)$$

$$c_s(R) = \frac{kT}{m_g}^{\frac{1}{2}} = 9.9 \cdot 10^4 \frac{R}{1\text{AU}}^{\frac{1}{4}} \frac{2.34}{2.34} \frac{1}{s} \quad (9)$$

$$H_g(R) = \frac{c_s(R)}{(R)} \quad (10)$$

where $g_0 = 1.7 \cdot 10^3 \text{ cm}^{-2}$ and $T_0 = 280\text{K}$. We will presume that $\sigma_d = g_0 \cdot 10^{-2}$, and $\sigma_{gg} = 10^{-15} \text{ cm}^2$ where σ_{gg} is the neutral gas-gas cross-section. The average gas molecule mass $m_g = m_H$ where $= 2.34$ is the mean molecular weight of the gas. The above values are presumed to remain constant in time.

2.3. Incorporating the role of disc turbulence and drag

As the dust grains grow, the effect of turbulence on their collisional velocity and scale height evolves. For dust grains smaller than the mean free path of the gas, that is $r_d < l_{\text{mfp}} = \frac{m_g}{\sigma_{gg} g}$, the gas-dust interaction is characterized by Epstein drag, whereas for $r_d > l_{\text{mfp}}$ we have Stokes drag (Landau & Lifshitz 1959). Throughout the paper we will use E and S as subscripts referring to behaviour with Epstein and Stokes drag respectively. For a dust grain interacting with a turbulent eddy of size λ and relative speed $v = v(0)$ at some initial time $t = 0$, the time evolution of v subject to Epstein drag is given by

$$\frac{dv}{dt} = -2 \frac{\rho_{\text{g}} \sigma_{\text{gd}} c_s}{m_d} v = -\frac{v}{E} \quad (11)$$

while for Stokes drag

$$\frac{dv}{dt} = -\frac{6 \rho_{\text{g}} r_d c_s}{m_d} v = -\frac{2 l_{\text{mfp}} \rho_{\text{g}} r_d c_s}{m_d} v = -\frac{v}{S} \quad (12)$$

where ρ_{g} is the gas density, $\sigma_{\text{gd}} = r_d^2$ is the gas-dust cross-section and $\lambda = \frac{g l_{\text{mfp}}}{3}$ chosen so that the drag equations are equal at the boundary between the Epstein and Stokes regimes $r_d = l_{\text{mfp}}$. We can combine the above two equations by writing

$$\frac{dv}{dt} = -\frac{v}{\tau}; \quad (13)$$

where $M_{\text{ax}}[s; E]$ and

$$E = \frac{m_d}{2c_s g_{\text{gd}}} = \frac{2}{3c_s \frac{g}{H_g}} = \frac{2}{3} \frac{g}{g} \quad (14)$$

and

$$s = \frac{2^2}{3l_{\text{fp}} g_d} : \quad (15)$$

We note that even though the gas is turbulent, the scale of the smallest turbulent eddy is generally larger than the scale of the dust grains during the growth phases we consider. This is why we do not use the high Reynolds number form (Landau & Lifshitz (1959)) of the Stokes drag (which varies as v^2 instead of as v). This will be justified a posteriori later.

Eqs. (11) and (12) have the same form whose solution is

$$v(t) = v(0)e^{-\frac{t}{E}} : \quad (16)$$

where again $M_{\text{ax}}(s; E)$ from (14) or (15). If $v(0) = v$, the turbulent velocity for an eddy of scale E , Eq. (16) shows that the dust grain will not exit the eddy in a time less than the eddy turnover time t . It follows that for $v(0) = v$ the dust grain will not exit the turbulent eddy until the eddy is destroyed. Upon being released from the eddy at its destruction, the grain's speed will have changed by

$$v(0) = v(0) \quad v(t) = v(0) \cdot 1 \cdot e^{-\frac{t}{E}} \quad , \quad v \cdot 1 \cdot e^{-\frac{t}{E}} : \quad (17)$$

As (17) is v_M for M (and assuming $v(0) = v_M$), Eq. (17) for M gives

$$v_M(0) = v_M \cdot 1 \cdot e^{-\frac{t_M}{E}} = \frac{p}{c_s} \cdot 1 \cdot e^{-\frac{1}{E}} \quad (18)$$

for the dust's random velocity with respect to the Keplerian disc, where the latter equality in (18) follows from (5) and (6).

3. Calculating the collisional and scale height velocities v_c and v_h

To facilitate incorporating the calculations of the previous sections into this and the following sections, we have collected key variables used in this paper into Table 1.

3.1. Collisional velocity of grains

To estimate the characteristic collisional velocity between two dust grains we assume that the grains' individual speeds are each v from (17), determined by having exited

separate eddies of comparable size. This assumption is straightforwardly justified if the turbulence is characterized by smaller scale eddies embedded fractally within larger scale eddies. If instead smaller scale eddies surround larger eddies, then justification of the above assumption follows from the Kolmogorov hypothesis that eddies of a given size cascade by interaction with eddies of comparable size and the fact that smaller eddies have lower speeds and less influence on a dust grain speed than a larger eddy. We then estimate the collisional velocity v_c as the average relative speed of dust grains from head-on and catch-up collisions:

$$v_c(0) = \frac{1}{2} (v(0) + v(0)) + \frac{1}{2} (v(0) - v(0)) = v(0) = v = 1 - e^{-\frac{t}{\tau}}; \quad (19)$$

where the latter equality follows from (17). Since v represents a linear combination of two dust grain speeds, and both sides of (11) and (12) above are linear, we then know from (19) (16) that v_c evolves as

$$v_c(t) = v_c(0)e^{-\frac{t}{\tau}} = v = 1 - e^{-\frac{t}{\tau}} - e^{-\frac{t}{\tau}}; \quad (20)$$

Averaging (20) over an eddy turnover time from $t=0$ to t then gives

$$v_c(x) = \frac{1}{t} \int_0^x v_c(t) dt = \frac{v}{x} = 1 - e^{-x^2} \quad (21)$$

where $x = \frac{t}{\tau}$. For a Kolmogorov turbulent spectrum, $v = v_M \frac{1}{x}^{-\frac{1}{3}}$ and $= v \tau$ which we can use with (5) and (6) to write:

$$v = (x)^{\frac{1}{2}} c_s^p; \quad (22)$$

Using this in (21) gives

$$v_c(x) = (x)^{\frac{1}{2}} \frac{(1 - e^{-x^2})^p}{p x} c_s^p; \quad (23)$$

We now derive expressions for $v_c(x)$ that apply for 3 separate regimes of x .

3.1.1. Maximum of $v_c(x)$

From (23) maximizing $v_c(x)$ gives

$$\text{Max}[v_c(x)] = v_{c,2} = B c_s^p \quad (24)$$

with $B = 0.53$ and the maximum occurs at $x = x_{\text{max}} = 2.3$. As long as there exists a for which $x = x_{\text{max}}$ we will use (24) as the turbulence induced collisional velocity. However, $t_M > t > t_m$ where $t_M = \frac{H_{\text{fp}}}{c_s^p} = \frac{1}{\tau}$ is the turnover time for the largest scale eddy and

$t_m = \frac{1_{\text{fp}}}{3 c_s^p}^{\frac{1}{2}}$ for the smallest. We will therefore need to treat the values of x where x cannot equal x_{max} separately.

3.1.2. Small case

For small enough x , the minimal value of $x = \frac{t_m}{t} > x_{\max}$ and we cannot use (24). However for such large x , $(1 - e^{-x})^2$ is close to 1 and we can approximate (23) as:

$$v_c(x) = v_{c,1}(x) \quad \frac{1}{x} \frac{p}{c_s} = \frac{1}{t_m} \frac{p}{c_s} : \quad (25)$$

This approximation is useful because the time scales of the regimes where we will use it are only weakly dependent on their initial length scales.

For sufficiently small values of x , the values of v_c from (25) will be less than the dust's thermal speed. For such grains we then just use the dust thermal velocity for v_c ,

$$v_c = v_{c,0}(x) = v_{c,th}(x) \quad c_s \frac{r}{m_d} = \frac{s}{\frac{3}{4} \frac{m_g}{m_d}} : \quad (26)$$

where m_g is the molecular weight of the gas.

3.1.3. Large case

For large x , the maximal value of $x = \frac{t_m}{t} = \frac{1}{e} < x_{\max}$ and again we cannot use (24). In this regime we have

$$v_c = v_{c,3} \quad v_M \frac{1}{x} 1 - e^{-x/2} = c_s \frac{p}{c_s} = 1 - e^{-1/2} : \quad (27)$$

3.1.4. Maximal $v_c(x)$

Equations (25), (24) and (27) allow us to maximize v_c with respect to x . We find

$$\text{Max}[v_c(x)] = v_c; \quad C \frac{p}{c_s} = 1 - e^{-1/2} \quad (28)$$

for $C = 0.407$ at $x = 1.26 < x_{\max}$. Accordingly, the maximum $v_c(x)$ occurs in the regime for which $v_c = v_{c,3}$.

3.2. Scale height velocity v_h

In addition to affecting v_c , turbulence also affects v_h by preventing settling. We can use (13) to calculate the settling time of a dust grain in the disc. Ignoring turbulence for the

moment, a grain at height z above the midplane moving towards the midplane with speed $v = \frac{dz}{dt}$ feels a vertical force

$$\frac{d^2z}{dt^2} = -\frac{GM}{R^2} \frac{z}{R} - \frac{1}{dt} \frac{dz}{dt} \quad (29)$$

which gives a terminal velocity (when $\frac{d^2z}{dt^2} = 0$) of

$$\frac{dz}{dt} = -\frac{GM}{R^3} z = -\frac{1}{2} z^2 : \quad (30)$$

Accordingly, $z(t) = z(0)e^{-\frac{t}{t_s}}$ where the settling time $t_s = (2)^{-1}$. We write $h = vt_s$ as the height reached by dust in one settling time.

We now incorporate the turbulence and obtain approximate expressions for v_h in (3) for different regimes. If the ratio of the settling time to the turnover time of the largest scale turbulence, $t_s < 1$, then the scale height cannot fall below the distance a single eddy can carry the dust from the midplane of the disc as the grains will spend more time inside eddies rather than settling. Indeed if $h < v_M = (c_s) =$, then $t_s < 1$, so we have from (18)

$$v_h = v_{h,3} \quad v_M = c_s^{\frac{p}{p-1}} e^{-\frac{1}{p-1}} : \quad (31)$$

In writing v_h in (31) we have used the fact that (17) is maximized for the largest eddies ($= M$), so we used v_M from (18) as the dust random velocity with respect to the Keplerian disc, and $^{-1}$ as the relevant eddy turnover time. If $t_s > 1$, then the approximation of isotropic turbulence will break down when the dust nears the top or bottom of the gas disc, limiting the scale height of the dust to that of the gas. If $h > H_g = c_s = (v_M) =$ then indeed $t_s > 1$, and we have the limiting value

$$v_h = v_{h,1} \quad c_s : \quad (32)$$

Note however, that for intermediate values of t_s for which both $t_s > 1$ and $H_g > h > \frac{v_M}{c_s}$ apply, the dust scale height $H_d = h$ and then

$$v_h = v_{h,2} = h = v_M t_s = \frac{c_s^{\frac{p}{p-1}}}{1 - e^{-\frac{1}{p-1}}} : \quad (33)$$

The period when $v_{h,2}$ from (33) holds begins when $= \frac{p}{p-1}$ and ends when $= 1$. Except near the end of that period, v_h and hence H_d vary as $^{-1}$. When $< < 1$ (in which case $v_{h,3}$ from (31) applies), $e^{-\frac{1}{p-1}} < 1 < \frac{1}{p-1}$ and so H_d again behaves as $^{-1}$. We consider the period of $\frac{p}{p-1} < < 1$ to be the first settling phase in which the dust may still interact with the gas disc as a whole, and > 1 to be the second settling phase in which the dust disc only interacts with the gas at the midplane of the disc. These phases are particularly important to distinguish when we consider the case of a disc with a dead zone.

In our calculations of $v_{h,2}$ and $v_{h,3}$, we have implicitly assumed that the grain growth time scale is longer than the settling time scale. If we calculate the growth time scale τ_g and the settling time τ_s at the beginning of settling ($\tau_g = \tau_s$), for Epstein drag we find that the settling time is shorter by a factor of $\frac{2cB}{3} \frac{1}{\frac{4}{3} - \frac{a}{g}}$. For $a > 10^{-8}$ our assumption is justified.

4. Collecting the grain growth formulae for specific regimes of v_c and v_h

In the previous sections we have derived a progression of four formulae for v_c and three for v_h that apply as dust grains grow. As long as the dust grows monotonically, for any values of R and a we have a progression of up to six regimes for $\frac{v_c}{v_h}$ and hence (3). As long as R and a remain in the ranges considered by this paper ($2 \times 10^{-6} < a < 10^{-2}$ and $0.5 \text{ AU} < R < 8 \text{ AU}$), Table 2 summarizes the regimes which we label by $i:j$ where i corresponds to $v_{c,i}$ and j corresponds to $v_{h,j}$. As our time scale calculations involve ratios of v_c and v_h we can see that once the grains begin to settle (regime 2.2. and higher), the factors of a will cancel in Eq. (3). However, as seen in Table 2, the grain size range over which the regimes occur still depends on R because the beginning and conditions for each regime depend on R . Thus the time scale for each regime, and the overall growth time to the gravitational instability phase still depends on R .

4.1. Regime 0:1

In this regime we have $v_h = v_{h,1} = c_s$ from (32) and $v_c = v_{c,0} = v_{th} = \frac{q}{m_d} c_s$ from (26). Here the dust motion is sufficiently strongly coupled to the bulk motion of the gas that the turbulent eddies have only the effect of preventing settling. Accordingly, (3) becomes

$$\frac{d}{dt} = c_d \frac{r \frac{m_g}{m_d}}{d} = \frac{r}{d} \frac{\frac{3m_g}{4} d}{d} : \quad (34)$$

Solving (34), the time scale $t_{0:1}(f)$ for regime 1 to grow dust grains from i to f is:

$$t_{0:1}(f; i) = \frac{4}{5c} \frac{r}{d} \frac{1}{\frac{3m_g}{4} \frac{d}{d}} \frac{f^{\frac{5}{2}} - i^{\frac{5}{2}}}{d} = \frac{4}{5} \frac{r}{3m_g} \frac{1}{d} \frac{f^{\frac{5}{2}} - i^{\frac{5}{2}}}{d} = t_{0:1}(f) : \quad (35)$$

Because the growth rate in this regime falls off strongly with grain size, the time spent in the regime depends only on its final size. This allows us to neglect any uncertainty in the initial radii of interstellar dust (which we will therefore approximate to be 0). We can also see that, as suggested in Sec. 2.1, the actual size dust grains can reach in regime 0:1 is strongly limited by time because $t \propto \frac{5}{2}$.

For the parameters we consider, regime 0:1 will lead into regime 1:1 and thus the former ends when $v_{c,0} = v_{c,1}$, after which $v_c = v_{c,1}$. Setting v_c from (26) and (25) equal we can see that this occurs for

$$f = 0:1;E \quad \frac{27m_g^2 d^2 t_m}{16}^{\frac{1}{5}} \quad (36)$$

for Epstein drag and for

$$f = 0:1;S \quad \frac{27m_g l_m^2 f_p^2 g^4 d^4 t_m}{16}^{\frac{1}{7}} \quad (37)$$

for Stokes drag.

4.2. Regime 1:1

When (25) is the dominant value for v_c and the dust is too small to settle ($v_h = v_{h,1}$ from (32)) we are in regime 1:1. As the dust grows in this regime, v_c is dominated by the smallest scale turbulent eddies, approaching the corresponding eddy speed.

Solving (3) in this regime we find the time scale $t_{1:1}(i; f)$ to grow the grains from i to f is

$$t_{1:1;E}(i; f) = \frac{3}{2c} \frac{g}{d} \frac{r}{t_m} \ln \frac{f}{i} \quad (38)$$

for Epstein drag and

$$t_{1:1;S}(i; f) = \frac{3}{2c} \frac{g l_m f_p d}{d} \frac{r}{t_m} \frac{1}{i} \frac{1}{f} , \quad \frac{3}{2} \frac{g l_m f_p d}{d} \frac{r}{t_m} \frac{1}{i} \quad (39)$$

for Stokes drag. Note that these values for $t_{1:1}$ are not strongly dependent on f , allowing us to use the approximations implicit in (25).

Once the damping time grows long enough such that

$$= \frac{t_m}{x_{max}} \quad (40)$$

then $v_c = v_{c,2}$ (24) applies and the regime 1:1 progresses to regime 2:1. This occurs for

$$f = 1:1;E \quad \frac{3}{2} \frac{g}{d} \frac{t_m}{x_{max}} \quad (41)$$

with Epstein drag and for

$$f = 1:1;S \quad \frac{3}{2} \frac{l_m f_p g}{d} \frac{t_m}{x_{max}}^{\frac{1}{2}} : \quad (42)$$

with Stokes drag.

4.3. Régime 2.1

In régime 2.1, the dust grows to couple with progressively larger and larger scale eddies that determine the collisional velocity v_c . For the range of r and R that we consider, the grains still remain small enough to avoid settling. (For smaller r and larger R , even the largest eddies would be too weak to prevent settling and an additional Régime 1.2 would occur.)

In régime 2.1, we have $v_{c,2}$ from (24) and $v_{h,1}$ from (32). Solving (3) we find the growth time scale in this régime to be

$$t_{2.1,E}(i; f) = \frac{r}{c_d B} \frac{1}{\frac{6}{f} \frac{1}{i^{\frac{1}{2}}}} , \quad \frac{r}{c_d B} \frac{1}{\frac{6}{f} \frac{1}{i^{\frac{1}{2}}}} \quad (43)$$

for Epstein drag and

$$t_{2.1,S}(i; f) = \frac{r}{\frac{34_m f p}{2} c_d B} \frac{1}{\ln \frac{f}{i}} \quad (44)$$

for Stokes drag.

Régime 2.1 progresses to régime 2.2 when the grains grow large enough that the turbulence can no longer prevent settling at which point (33) applies. This occurs for

$$p - \frac{p}{2} = \frac{p}{2} \quad (45)$$

Accordingly Régime 2.1 ends for

$$f =_{2.1,E} \frac{3^{\frac{p}{2}} - \frac{p}{2}}{c_d B} \quad (46)$$

with Epstein drag and for

$$f =_{2.1,S} \frac{3^{\frac{p}{2}} - \frac{p}{2}}{\frac{34_m f p}{2} c_d B} \quad : \quad (47)$$

with Stokes drag.

4.4. Régime 2.2

Régime 2.2 occurs for dust grains large enough to begin settling out of the gas disc and also have their collisional velocity determined by coupling to non-microminum scale turbulence.

Here we use $v_{c,2}$ from (24) and $v_{h,2}$ from (33) while approximating $1 - e^{-\frac{1}{2}} = 1$. Solving (3) we find the time scale to grow from some i to f in this regime to be

$$t_{2,2,E} (i; f) = \frac{2}{c_d B} \frac{3}{2} \frac{g}{2}^{\frac{3}{2}} i^{\frac{1}{2}} f^{\frac{1}{2}}, \quad \frac{2}{c_d B} \frac{3}{2} \frac{g}{2}^{\frac{3}{2}} i^{\frac{1}{2}} \quad (48)$$

with Epstein drag and

$$t_{2,2,S} = \frac{1}{2c_d B} \frac{3l_{mfp} g_d}{2}^{\frac{3}{2}} i^2 f^2, \quad \frac{1}{2c_d B} \frac{3l_{mfp} g_d}{2}^{\frac{3}{2}} i^2 \quad (49)$$

Regime 2.2 ends when the turbulent length scale on which the dust's collisional velocity depends reaches the largest turbulent scale. This happens when $x = \frac{t_m}{v} = x_{max}$, which occurs for

$$= \frac{1}{x_{max}} : \quad (50)$$

Accordingly, we find that in the Epstein regime, regime 2.2 ends for

$$f = t_{2,2,E} \frac{3}{2x_{max}} \quad (51)$$

and

$$f = t_{2,2,S} \frac{3l_{mfp} g_d}{2x_{max}}^{\frac{1}{2}} \quad (52)$$

in the Stokes regime. None of (48), (49), (51) or (52) depend on so the only dependence of the time scales that result from regime 2.2 derives from the initial size condition that determines when the regime applies.

4.5. Regime 3.2

In regime 3.2 we use $v_{c,3}$ from (27) while continuing to use $v_{h,2}$ from (33). The dust is decoupling from the turbulence but has yet to reach the last settling phase. Writing (3) in this regime we find

$$\frac{d}{dt} = c_d^{3/2} 1 - e^{-\frac{1}{2}} \cdot c_d^{3/2} 1 - e^{-1} \quad (53)$$

as regime 3.2 will end when $= 1$. Using the above approximation we find that the time scale to grow from some i to f in the regime is less than

$$t_{3,2,E}, \frac{9}{4c_d} \frac{g^2}{(1 - e^{-1})} i^1 f^1, \quad \frac{9}{4c_d} \frac{g^2}{(1 - e^{-1})} i^1 f^1 ; \quad (54)$$

for Epstein drag and

$$t_{3.2;E} = \frac{3 \frac{2 l_m^2 f p}{g} \frac{d^2}{d}}{4 c_d (1 - e^{-1})} \quad i^3 \quad f^3, \quad \frac{3 \frac{2 l_m^2 f p}{g} \frac{d^2}{d}}{4 c_d (1 - e^{-1})} \quad i^3 \quad f^3 \quad (55)$$

for Stokes drag.

Regime 3.2 ends when the dust is no longer buoyed by multiple turbulent eddies but instead settles after each encounter with an eddy. This happens when $H_d = h = v t_s = \frac{v}{f}$ which occurs for

$$= \quad 1 : \quad (56)$$

Accordingly we find that for Epstein drag regime 3.2 ends for

$$f = \tau_{3.2;E} = \frac{3 g}{2} \quad (57)$$

and for Stokes drag is ends for

$$f = \tau_{3.2;S} = \frac{3 l_m f p g d}{2}^{\frac{1}{2}} : \quad (58)$$

We can see that regime 3.2's time scales do not depend on f in any fashion.

4.6. Regime 3.3

In this final regime 3.3, we use $v_{c,3}$ from (27) and $v_{h,3}$ from (31). Here the dust has entered its final settling phase. While (3) is not simply solvable in this regime, the large (small x) limit of $\frac{v_c}{v_h} = \frac{1 - e^{-x}}{x}$ is 1, for large enough dust grains. The large x approximation greatly simplifies (3) and results in time scale predictions that are accurate to around 10 percent. We therefore incorporate the approximation as an analytic guide to the behaviour of the regime and see that the growth duration from (3) is then

$$t_{3.3} (i; f) = \frac{1}{c_d} (f - i) + \frac{1}{d} f : \quad (59)$$

The large x approximation underestimates the time scales of regime 3.3 so in our growth time scale plots we have solved (3) numerically, but the comparison is shown in Fig. (7).

Regime 3.3 ends when the dust disc becomes gravitationally unstable, which occurs when the Toomre criterion (Binney & Tremaine 1987)

$$v_h = \frac{-G}{2} \frac{d}{d} \quad (60)$$

is satisfied. While given our parameter use the above condition is natural, much of the prior work writes this condition in terms of the dust disc density ρ , which is related to v_h by $\rho \propto v_h^{-1}$. Substituting $1 - e^{-x} \approx x$ into (31) we find

$$= \frac{2^{\frac{p}{2}} - c_s}{G \frac{d}{d}} : \quad (61)$$

Regime 3:3 then ends when

$$f'_{3:3:E} = \frac{3^{\frac{p}{2}} - c_s}{G \frac{d}{d}} - \frac{g}{d} \quad (62)$$

for Epstein drag and when

$$f'_{3:3:S} = \frac{3^{\frac{p}{2}} - l_{\text{fp}} c_s}{G \frac{d}{d}} - \frac{g}{d}^{\frac{1}{2}} \quad (63)$$

for Stokes drag. While we used the exact velocity formulas in our numerical integrations of (3) to calculate $t_{3:3}$, the latter 3 approximations provided the upper bound of the integral as well as the analytic calculation of Fig. (7). For smaller values of x (and thus larger final values of x) the approximation $1 - e^{-x} \approx x$ overestimates our final and thus overestimates the duration of regime 3:3.

4.7. Regime ordering and the applicability of Table 2.

Before discussing the quantitative results, we comment on the ordering of the regime progression summarized in Table 2. As long as $x_{\text{max}}^2 < 1$, then $- \frac{1}{x_{\text{max}}} < \frac{1}{x}$. It follows that the transition from $v_{h,1}$ to $v_{h,2}$ will occur before that from $v_{c,2}$ to $v_{c,3}$ which in turn will occur before that from $v_{h,2}$ to $v_{h,3}$. For large grains, a possible deviation from the bottom-to-top canonical ordering shown in Table 2 arises if gravitational instability is triggered before $v_{h,3}$, which for $0.5 \text{ AU} < R < 8 \text{ AU}$ requires $\frac{t_m}{x_{\text{max}}} > 3 \times 10^{-8}$. For small grains, possible deviations from the canonical regime ordering occurs when $\frac{t_m}{x_{\text{max}}} = \frac{1}{x}$ (Sec. 4.3) and when equations (36), (37) hold for $\frac{t_m}{x_{\text{max}}} > 1$. In this case, the weakness of the turbulence delays the transition from thermal collisions to turbulent collisions. For $0.5 \text{ AU} < R < 8 \text{ AU}$ no changes from the canonical regime ordering occur for $2 \times 10^{-6} < \frac{t_m}{x_{\text{max}}} < 1$.

It follows that as long as we restrict ourselves to $2 \times 10^{-6} < \frac{t_m}{x_{\text{max}}} < 10^{-2}$ the ordering in Table 2 will hold for $0.5 \text{ AU} < R < 8 \text{ AU}$. As $\frac{t_m}{x_{\text{max}}}$ drops below about 10^{-6} our present regime ordering of Table 2 breaks down, though a new ordering could be constructed.

5. Results for growth time scales and sizes

5.1. Grain sizes at the end of each regime

Figures 1 and 2 show the grain sizes calculated from the formulae for f for the end of each regime of the previous section as a function of disc location. The calculations use a fixed $d = 1\text{cm}^3$, so $r_d = r_d(\rho) / \rho$. The regimes are labeled in the Figure captions. The solid line is the curve d_{mfp} , which represents the boundary between Stokes (left) and Epstein (right) drag regimes.

An important feature of Figs. 1 and 2 is that there is a maximum grain size in each regime which falls along the line bounding the Stokes and Epstein drag regimes. This arises because all of the equations for f of the previous sections that define the boundaries between regimes are increasing functions of R for Stokes drag and decreasing functions of R for Epstein drag. Because the drag viscosities are equal at the boundary between Stokes and Epstein regimes (Sec. 2.3), for each regime of Sec. 4, there is a triple point in the plots of f vs R where $\epsilon = s = d_{\text{mfp}}$. The triple point is formed by the intersection of the curves corresponding to Epstein and Stokes drags, and the line which represents this boundary as a function of R . Compared to the Stokes regime, the Epstein regime curve is less dependent on the various parameters such as d and d_{mfp} .

The triple point of regime 3.2 is particularly significant because the boundary between regime 3.2 and 3.3 defines the grain size scale for which grain infall from the drag on the gas is important (discussed in Sec. 6.2.1). For our disc model this triple point is independent of d and is given by

$$R_{\text{tp}} = 6.14 \frac{g_0}{1.7 \cdot 10^3 \text{cm}^2} \frac{d}{1\text{cm}^3}^{1/7} \text{AU} : \quad (64)$$

While we first present results without including dust migration, note that due to the monotonic behaviour of the boundaries in a given drag regime, inward migration would cause grains of a constant size to rise above the size curves of Figs. 1 and 2 in the Stokes regime but fall below the curves in the Epstein regime. As a grain grows from the smallest to the largest within a regime, it will experience Epstein drag for R above the triple point of the regime, Stokes drag if R is less than the triple point of the prior regime, and it will transit from Epstein to Stokes drag if R lies between the two triple points. Figures 1, 2 and 3 show that because of this behaviour, the peak grain size occurs for $5 < R < 8\text{AU}$ for dust grains of $r_d = 1\text{cm}^3$.

Fig. 3 shows specifically the grain size at which gravitational instability occurs as a function of radius computed from section 4.7. This represents the maximum size attained

through all the regimes 0:1 through 3:3, and the size after which gravitational instability physics not included in the present work takes over.

5.2. Total time scales to grow to gravitationally unstable regime

Figs. 4, 5, 9, 10, 11, 12 and 13 show the total time scale t_T to grow through all regimes 0:1 through 3:3 and thus the total time to reach the gravitationally unstable phase.

A key feature to note is the dependence of t_T , as exemplified in Figs. 4 and 5. For regimes 0:1 through 2:2, the time spent in a given regime is a decreasing function of R . The duration of regime 3:2 is independent of R and that of regime 3:3 is an increasing function of R . It follows that for any given R there will be an η that minimizes t_T . For $R = 3\text{AU}$ this value is $\eta = 3 \times 10^{-2}$ while for $R = 8\text{AU}$ it is $\eta = 10^{-3}$. Provided η and R are within the range described in Sec. 4.8, this allows us to determine the minimum and maximum values of η for which the total growth through all regimes is less than the observationally constrained time scale ($< 10^6$ yr) of planetesimal formation.

Figs. 10, 11, 12 and 13 are analogous to Figs. 4 and 5 but for different dust grain material densities and dust/gas surface densities in the disc (see Fig. captions).

By using the variable η in equation (3), the fact that in the Epstein regime the dust density and gas mean free path effect neither the peak collisional velocities nor the time scales of the regimes other than 0:1 falls from eq. (14) along with the various time scale equations (38) etc... However, the mass and radius of the grains vary as $\eta^{2/3}$ or $\eta^{1/3}$ at various stages of the evolution so the actual grain radii at which the regime transitions occur do vary. In the Stokes regime, density plays a non-trivial role in the effects of turbulence on the grain trajectory (15) and therefore in determining the boundary between the two drag regimes as well as the details of the regimes of $\frac{v_c}{v_h}$. In figures 10 and 11 we plot the time scales for η of 5 and $0.5\eta_{\text{min}}^{-3}$.

From (3), we see that increasing the dust disc surface density η_d will decrease the growth time scale. However, in our equations η_d frequently appears in a ratio with η_g . The effect of changing η_d while keeping η_g constant is greater than that of changing both equally, as can be seen in Figs. (12) and (13). The total surface density primarily affects the condition for gravitational instability which determines the time spent in regime 3:3. This dominates the growth time scale at large R . Changing the dust surface density alone has a strong influence throughout the disc.

5.3. Dead zones reduce the total growth time

The MRI (Balbus & Hawley 1991) may be the primary source of turbulence in a protoplanetary disc but the entire gas disc need not be sufficiently ionized for the instability to occur. The MRI-stable region of the disc is labeled a dead zone (Matsumura & Pudritz (2005), Sano et al. (2000)) and will have a smaller value for than the live zone. If there is a dead zone for approximately the scale height over some range of R , then we can simply treat the live and dead zones as having separate values of and merging them in our radially dependent calculations, while noting that dust unable to decouple from the turbulence on a viscous time scale could be deposited at the outer edge of the dead zone.

If instead we consider a turbulent disc with a dead zone near the midplane of the disc (with a height H_d) for some range of R (but live for a significant thickness above the midplane) we can approximate the growth time scales by using the not-fully-settled regimes (0:1 through 3:2) for the live zone and its value of , while assuming the settled regime 3:3 lies within the dead zone evolving with that region's . The scale height of the dust at the beginning of regime 3:2 is $2^{p-1}H_g$ which will likely lie within the dead zone but the time scale of regime 3:2 does not depend on . We expect that the dead zone will actually lie within regime 2:2 but the only dependency of that regime's time scales lies with the initial size condition, which occurs when $H_d = H_g$, within the live zone. It follows that assuming regimes 3:3 is the only one within the dead zone will give the correct time scale. Note that the scale height of the dust, $H_d = 0.5H_g$ for roughly

$$= \frac{2^{p-1}}{2} : \quad (65)$$

within regime 2:2 of Sec. 4.4. The time scale behaviour with a dead zone is important because the duration of regime 3:3 is an increasing function of , whereas regimes 0:1 through 2:1 are decreasing functions of . Regime 2:2's time scale, as discussed above, will only depend on the live zone . Accordingly, as the contrast between the values of in the live and dead zones increase, the the total time for planetesimal growth decreases. In particular, therefore, having a dead zone as opposed to no dead zone, decreases the total time below that of a disc with only one of the two values of .

The role of a dead zone in lowering the growth time scale is shown in Fig. (9).

6. Discussion

6.1. Range of v_c and R for which gravitational instability can occur

Armed with equations for growth rates and collisional velocities of the dust grains, we can identify the range of values of v_c that will permit planetesimal growth in a realistic turbulent disc on observable time scales.

While we are restricted by our regime definitions and regime ordering to values of 10^{-6} , the effect of α on the estimated time scales for planetesimal growth is pronounced. We now discuss the effect of α and c_s on the range of values that allow for planetesimal formation on the observationally relevant time scales.

6.1.1. Constraints implied by the maximum v_c

We can place a maximum value for v_c that still allows planetesimal formation by studying its influence on the maximum collisional velocity. We have used only the simple sticking parameter c to characterize the extent of sticking between interacting dust grains. However, for large enough values of v_c , the dust grains will destroy each other on impact. A more complete dust grain interaction model would allow us to constrain v_c and thus because the maximum v_c varies as α^{-p} from (28). For a disc with a dead zone, the maximum collisional velocity in the dead zone will be lower than that in the live zone because of the lower value of α . This helps facilitate planet formation even if the live zone is otherwise too large. We quantify this below.

If the end of regime 3.2 appropriately marks the transition to the dead zone region, then $\alpha = 1$ and from (28)

$$v_{c,\max} = \alpha^{-p} c_s = 1^{-p} c_s = 0.4^{-p} c_s; \quad (66)$$

for a dead zone height of

$$H_D = (v_{h,3} = c_s) H_g = \alpha^{-p} H_g = 1^{-p} H_g = 0.4^{-p} H_g; \quad (67)$$

from (33).

If instead the end of regime 2.2 defines the beginning of the dead zone, then from (24) and (50) we have

$$v_{c,\max} = \frac{r}{x_{\max}} B c_s = 0.35^{-p} c_s; \quad (68)$$

and a dead zone height from (33) and (50) of

$$H_D = (v_{h,2} = c_s) H_g = \alpha^{-p} x_{\max}^{-1} e^{-x_{\max}} H_g = 2^{-p} H_g; \quad (69)$$

If the dead zone is taken to be vertically sandwiched between live zones, and the height of the former is roughly half that of the gas disc, then (65) gives the condition for the dead zone height to equal the dust scale height. The maximum live zone collisional velocity occurs for that value of α and is

$$v_{c, \text{max}} = \frac{p}{2} \frac{3}{4} B c_s, \quad 0.75 \frac{3}{4} c_s; \quad (70)$$

We plot results for live zone values of $\alpha = 10^{-3}$ and $\alpha = 10^{-4}$ in Fig. (6). The maximum collisional velocities occur for dust grains of centimeter to meter scales. The top solid line in each panel represents the maximum collisional velocities in the live zone and the bottom solid line represents the maximum collisional velocities for the dead zone. From common experience, we infer that it is unlikely for dust grains colliding with speeds $> 30 \text{ km/h}$ to stick from the collision (and more likely that they obliterate). Therefore we interpret Fig. (6) to imply that, while for a live zone near or above 10^{-3} , a significant dead zone (with a lower $\alpha = 10^{-4}$) is needed in order to avoid the collisional destruction and enable planet formation in the absence of additional processes like vortices. However, if the live zone were as low as 10^{-4} then a dead zone would be unnecessary.

Our results are consistent with Youdin (2004) who finds limits for v_c near 5 m s^{-1} , 18 km s^{-1} from the physics of dust grain collisions.

6.1.2. Constraints implied by the total growth time scale through regime 3.3

The discovery of a planet younger than a million years old (D'Alessio et al. 2005) requires, at minimum, that planetesimals grow to the gravitational unstable phase on a time scale substantially shorter. For $R = 3 \text{ AU}$ and $c = 1$ our total growth time scale to reach this phase, t_g , satisfies $t_g \leq 10^4 \text{ yr}$ for $10^{-3} < \alpha < 10^{-4}$, allowing at least an order of magnitude leeway while still staying well below 10^6 yr (Fig. 4). We also see that as α falls below 10^{-4} the total time scale rapidly rises. This allows us to place a lower bound on α greater than the bound required by the validity (see Sec. 2.2) of our regime ordering in Table (2).

6.2. On the validity of key approximations

6.2.1. Constraints from comparing headwind induced infall and grain growth time scales

We have made the approximation that $v_d(R)$ and $v_g(R)$ are time independent and that dust grains do not migrate. However, while gas depleted by accretion is replenished from the outer regions of the disc or envelope, dust migration cannot be so simply ignored. The

gas in a protoplanetary disc is partially pressure supported and so rotates at a sub-keplerian velocity. The dust grains will then feel a headwind and begin to spiral in towards the star. As seen in Nakagawa et al. (1986), eq 1.9 (which omits a fraction sign)

$$v_{\text{orb},g} = (1 - \epsilon) v_K ; \quad (71)$$

where v_K is the Keplerian velocity and

$$= \frac{R^2}{2GM_g} \frac{dP}{dR} = \frac{13}{8} \frac{c_s^2}{R} \quad (72)$$

parametrises the difference between the gas orbit speed and the Keplerian speed. The gas disc also accretes viscously, with time scale $t = \frac{R^2}{c_s H_g}$ and accretion velocity $v' = \frac{c_s^2}{R}$. If we assume $\epsilon_g \gg \epsilon$, our ϵ^1 corresponds to the ϵ of Nakagawa et al. (1986), so adding in the viscous radial velocity we rewrite their eq 2.11 for the infall speed as

$$v_R = 2 \frac{R^2}{1 + (\epsilon)^2} \frac{c_s^2}{R} \frac{1}{1 + (\epsilon)^2} = v_r + v ; \quad (73)$$

where $v_r = 2 \frac{R^2}{1 + (\epsilon)^2}$ is due to the headwind and $v = \frac{c_s^2}{R} \frac{1}{1 + (\epsilon)^2}$ is due to the viscous accretion flow. Any violation of $\epsilon_g \gg \epsilon$ will only serve to slow the radial drift. For near ϵ^1 , $v' \approx 6 \times 10^6 \frac{\text{AU}}{10^3 \text{yr}} \ll v_r$. The maximum $v_R(\epsilon)$ is $R' \frac{1 \text{AU}}{89 \text{yr}}$ and occurs, for any R , at $\epsilon = \epsilon^1$, which is also the end of our regime 3.2. For $\epsilon \ll \epsilon^1$, $v_R \approx v_r$ while for $\epsilon \gg \epsilon^1$, $v_R \approx v$.

Migration can be ignored only if the deceleration time scale of the infall speed $v_R = v_R$ is less than the infall time scale $R = v_R$ for the most affected grains. For $\epsilon \gg \epsilon^1$, $v_R \approx v$ and the deceleration time scale can be written as $\epsilon = \frac{R}{v}$ for any drag regime. We can then cast the condition to ignore migration as the requirement that the ratio $\frac{\epsilon}{R = v_R} < 1$. In Fig. 14 we plot 1=c times this ratio. The jump in the plot at $R' = 6 \text{AU}$ is due to the fact that $\frac{s}{s} = \frac{1}{2}$ but $\frac{E}{E} = \frac{1}{2}$ and $R = 6 \text{AU}$ is the triple point of regime 3.2 (sec. 5.1) where the drag regime for the appropriately sized grains changes (as seen in Fig. 1). In Fig. 15 we plot the R inside of which the headwind infall can be ignored, as a function of c . It follows that infalling grains will pile up at this radius, leading to a disc dust density enhancement and opportunity for enhanced planetesimal formation. This in turn, allows more flexibility in the value range for c that still facilitates rapid planetesimal formation in the absence of other physics.

There is a subtlety however. As we can see in Fig. 1, inside of the regime 3.2 triple point (sec. 5.1, for our disc $R = 6 \text{AU}$), the curve $\epsilon = \epsilon^1$ marking the onset of regime 3.3 (second curve from the top in the right panel) lies within the Stokes drag regime, while for $R > 6 \text{AU}$ Epstein drag applies. In the Stokes regime, the curve is an increasing function

of R so as grains are transported inward, their w ill increase above 1 and regime 3.3 will always occur. For the Epstein drag regime however, the inward transport will keep the grains below the $= ^1$ curve; here if grain growth at a given radius is slower than the inward transport, the grain will never transit the curve, preventing the transition to the second settling regime 3.3 and thus forbidding the onset of gravitational instability.

To see whether this circumstance arises, we calculate the rate of change of c (where $c = \frac{3}{2} \frac{g}{2}$ is the critical size required to satisfy $e = ^1$) due to the radial transport and compare it to $\frac{dc}{dt}$ from Eq. (3). We find

$$\frac{dc}{dt} = \frac{d}{dt} \frac{3}{2} \frac{g}{2} = \frac{3}{2} \frac{c}{R} \frac{dR}{dt} = \frac{3}{2} c \frac{R}{c} = \frac{117}{36} \frac{g H^2}{R^2} \quad (74)$$

where g scales as $R^{-\frac{3}{2}}$ from (7) and

$$\frac{d}{dt} = c_d \frac{1}{e} \quad (75)$$

for grains with $= c$. For the disc model we have chosen in Sec. 2.2., we find

$$\frac{d}{dt} = \frac{d}{dt} \frac{R}{AU} \frac{1}{\frac{g}{100}} \frac{1}{e} : \quad (76)$$

where this quantity is less than 1 in the Epstein drag regime for the relevant grain sizes (which, for our canonical disc parameters, occurs everywhere in the Epstein regime, $r > R_{tp}$), the inward transport prevents the grains from growing to regime 3.3. Because the time scale to reach c is an increasing function of R while the total mass contained within an annulus of width dR is a decreasing function of R , changes in d as the dust falls inward do not alter the basic conclusion. Increasing g increases the triple point R_{tp} of (Eq. (64)) and increasing the ratio $g = d$ decreases the radius where (76) drops below unity. Thus the critical radius above which planetesimal growth is prevented is indeed R_{tp} . We plot the effect near $R = 6AU$ in Fig. (16) for our canonical disk parameters. The effect remains important if the basic disc parameters are altered, but the radius of the triple point and the critical radius where (76) drops below unity and the triple point radius (64) can change.

The important upshot of the effect just described is that gravitational instability cannot be easily reached at radii larger than the triple point (discussed in section 5.1) that arises in regime 3.2 without additional physics like vortices, or a significantly different disc model. It is interesting, if not unsurprising in hindsight, that the drag induced grain agglomeration benefit from vortices (Barge & Sommeria 1995) is maximized for the same $= ^1$ condition that gives the maximum infall speed we found from (73).

The conclusions drawn from (76) and the limits on c from Fig. (15) are essentially independent of e because its effects on v_c and v_h in Eq. (3) for the relevant regimes cancel.

This allows us to use Fig. (15) to constrain our sticking parameter, independent of (at least for $R < 8\text{AU}$). This makes our constraints more meaningful.

6.2.2. Neglect of gravitational enhancement to cross section

Our model ends at the point when gravitational instabilities take over. We have calculated whether gravitational enhancement to dust-dust collisions plays any role before that time. We find the effect to be small for all but the largest even for the largest scale dust. This is shown in Fig. 8.

6.2.3. Use of linear vs. quadratic in v drag forces

Even though the present flow is turbulent, the laminar approximation for the Stokes drag was used because the grains were presumed to be smaller than the smallest turbulent eddies at all times. Therefore, unlike a macroscopic object in a turbulent flow, the grain would see an effectively laminar flow.

This approximation can be justified a posteriori: It turns out that only very close to the star, do the largest scale dust grains just before gravitational instability become comparable to the smallest scale turbulence. We neglect the change in drag law that this would imply because those eddies are far less massive than the grains, are traveling at velocities nearly equal to these dust grains at the onset gravitational instability and so will have negligible effects on the grain trajectories.

6.2.4. Sticking

The most uncertain aspect of our model lies in the sticking mechanism. A value of $c = 1$, which represents 100% efficiency for collisions resulting in sticking, seems unlikely. Considering c to be a gestalt parameter combining both all the possible sticking and destruction results of collisions and examining (3) we can see that our time scale T depends inversely on c . Comparison with sec. 6.2.1 we see that decreasing c strongly decreases the outer value for R allowed by the headwind induced infall, although this will only become important if c nears 10^{-2} . If we had a well developed sticking model we could calculate the maximum collisional velocity before grain collisions result in destruction. Accordingly, our ability to constrain c , either through disallowing grain destruction through high velocity collisions or through time scale arguments is limited by the quality of the sticking model.

7. Conclusion

We have developed a simple model to estimate the effects of disc turbulence on planetesimal growth. We show that turbulence has two competing influences: (1) It increases the collisional velocity of dust grains which increases their interaction for growth. (2) It increases the velocity which determines the scale height of the dust layer in the disc which decreases the volume density lowering the interaction for growth. Since the growth rate of grains depends on the ratio of these two velocities, the evolution of protoplanetary formation depends on the evolution of this ratio. Because the coupling of the gas to the dust evolves with grain size, the ratio is not a constant. Our work differs from previous studies by explicitly incorporating the dynamical evolution of dust grain size and the dust settling and considering discs with and without dead zones.

We identify the range of turbulent strength, measured by c , the range of dust sticking efficiency, measured by c , and the disc radius range for which protoplanetary formation progresses to the gravitational instability phase on observationally constrained time scales ($< 10^6$ yr, D'Agostino et al. (2005)). The allowed ranges emerge from constraints on (1) the total time scale for planetesimal formation, (2) the infall time scale of the dust grains compared to their growth time and (3) the destruction of dust grains from high velocity collisions. We find that dust grain infall due to headwind gas drag prohibits reaching the gravitational instability phase outside a limiting radius that depends on the transition between Stokes and Epstein drag (the regime 3:2 triple point from Sec. 5.1. For our disc model this occurs at $R = R_{tp}$ given by Eq. (64). It is possible that material piles up at $R = R_{tp}$ which may enhance planetesimal growth at this radius. This latter effect requires further work.

For $R < R_{tp}$, we find that for $c > 10^{-2}$ and $> 10^{-3}$ turbulence does not catastrophically slow the needed planetesimal growth, as seen in Fig. (4), even though the time and size scales at which the growth occurs still depend strongly on those parameters. These results depend on the unknown physics of grain-grain interactions determining c , but the assumption that grain destruction results from collisions between $> 1\text{ cm}$ sized grains with velocities $> 30\text{ km/hr}$ strictly requires $c < 10^{-2}$ for all discs if growth is to be fast enough. As determined in Sec. 6.1.1, values of $c > 10^{-3}$ for discs with substantial dead zones and $c > 10^{-4}$ are acceptable.

The condition that the grain infall time be longer than the grain growth time (as discussed in section 6.2.1) also leads to an independent minimum acceptable c as seen in Fig. (16). We find that as c falls below $\frac{1}{10}$ the distance from the star at which gravitational instability can be reached and planetesimal formation occurs falls below 3 AU. For $c = 10^{-2}$ planetesimal formation won't occur outside of roughly 1 AU. Values of c below 10^{-2} are too low to produce rapid enough planetesimal growth in the absence of additional physics.

Although more detailed calculations with grain size spectra, collisional velocity spectra, and a more detailed grain-grain collision model are needed, our most robust conclusion is that planetesimal growth in an initially gravitationally stable turbulent disc is not prohibited by turbulence with $10^{-6} \text{ to } 10^{-3}$, even in the absence of including dust agglomeration enhancement mechanisms. For 10^{-2} we do not find much opportunity for growth, even for discs with a dead zone, and additional physics to promote dust growth such as large scale vortices, or the consequences of mass pile up at $R = R_{\text{tp}}$ need to be considered.

Acknowledgments: We acknowledge support from NSF grants AST-0406799 and AST-0406823, NASA grant ATP 04-0000-0016, and the KITP of UCSB, where this research was supported in part by NSF Grant PHY-9907949. AH acknowledges a H. Orton Graduate Fellowship from the Laboratory for Laser Energetics.

R E F E R E N C E S

Balbus, S. A., & Hawley, J. F. 1991, *ApJ*, 376, 214

Barge, P., & Sommeria, J. 1995, *A & A*, 295, L1

Barge, P., & Vinton, M. 2003, *ApJ*, 593, L117

Barranco, J. A., & Marcus, P. S. 2005, *ApJ*, 623, 1157

Binney, J., & Tremaine, S. 1987, *Galactic Dynamics*. Princeton Univ. Press, Princeton, NJ

Blackman, E. G. 2001, *MNRAS*, 323, 497,

Boss, A. P. 1997, *Science*, 276, 1836

Champane, J. M., Dobrovolskis, A. R., & Cuzzi, J. N. 1995, *Physics of Fluids*, 7, 1703

Chavanis, P. H. 2000, *A & A*, 356, 1089

Cuzzi, J. N., Dobrovolskis, A. R., & Champane, J. M. 1993, *Icarus*, 106, 102

D'Alessio, P., et al. 2005, *ApJ*, 621, 461

de Pater, I., & Lissauer, J. 2001, *Planetary Sciences*. Cambridge Univ. Press, Cambridge

Goldreich, P., & Ward, W. R. 1973, *ApJ*, 183, 1051

Hartmann, L. 1998, *Accretion processes in star formation*. Cambridge Univ. Press, Cambridge

Ishitsu, N., & Sekiya, M. 2003, *Icarus*, 165, 181

Landau, L. D., & Lifshitz, E. M. 1959, *Fluid Mechanics. Course of theoretical physics.* Pergamon Press, Oxford

Matsumura, S., & Pudritz, R. E. 2005, *ApJ*, 618, L137

Nakagawa, Y., Sekiya, M., & Hayashi, C. 1986, *Icarus*, 67, 375

Sano, T., Miyama, S. M., Umebayashi, T., & Nakano, T. 2000, *ApJ*, 543, 486

Shakura, N. I., & Sunyaev, R. A. 1973, *A & A*, 24, 337

Voelk, H. J., Morfill, G. E., Roeser, S., & Jones, F. C. 1980, *A & A*, 85, 316

Wiedenschilling, S. J. 1980, *Icarus*, 44, 172

Wunsch, R., Klahr, H., & Rozyczka, M. 2005, *MNRAS*, 362, 361

Youdin, A. N. 2004, ASP Conf. Ser. 323: Star Formation in the Interstellar Medium : In Honor of David Hollenbach, 323, 319

Youdin, A. N., & Chiang, E. I. 2004, *ApJ*, 601, 1109

Table 1. Key Variables

Variable	Description
d	Dust disc density
g	Dust grain density
d	Gas disc density
g	Dust disc surface density
g	Gas disc surface density
g_0	Gas disc surface density at $R = 1\text{AU}$
r_d	Grain radius
m_d	Grain mass
m_g	Mass of a gas molecule
v_{th}	Dust thermal speed
E	Grain frictional stopping time for Epstein drag
s	Grain frictional stopping time for Stokes drag
	Keplerian angular velocity
H_g	Gas disc scale height
H_d	Dust disc scale height
H_D	Dead zone height
c_s	Gas sound speed
c	Sticking parameter
	Shakura-Sunyaev viscosity parameter
σ_{gg}	Neutral gas collisional cross-section
σ_{gd}	Dust-gas collisional cross-section
σ_{dd}	Grain-grain collisional cross-section
R	Distance from the star
t_T	Total time scale to achieve gravitational instability

Table 2. Regime Descriptions and Ordering

Regime	Start Condition	End Condition	Collisional Velocity	Height Velocity
Regime 3:3	$= \frac{1}{\infty}$	$= \frac{2 \frac{p - c_s}{G_d}}{1}$	$p - c_s$	$1 \cdot e^{-\frac{1}{2}}$
Regime 3:2	$= \frac{1}{x_{\max}}$	$= \frac{1}{\infty}$	$p - c_s$	$1 \cdot e^{-\frac{1}{2}}$
Regime 2:2	$= \frac{p -}{\infty}$	$= \frac{1}{x_{\max}}$	$\frac{p}{B c_s}$	$\frac{p - c_s}{c_s} \cdot 1 \cdot e^{-\frac{1}{2}}$
Regime 2:1	$= \frac{t_m}{x_{\max}}$	$= \frac{p -}{\infty}$	$\frac{p}{B c_s}$	c_s
Regime 1:1	Eq. (36), (37)	$= \frac{t_m}{x_{\max}}$	$\frac{q}{t_m} \cdot c_s$	c_s
Regime 0:1	Interstellar Dust	Eq. (36), (37)	$q \frac{\frac{3}{4} \frac{d_m g}{c_s^3}}{c_s}$	c_s

Note. | The planetesimal growth regimes that occur in our model which progress from bottom to top as the dust grains grow. The collisional velocities are developed in equations (26), (25), (24) and (27) and the height velocities in (32), (33) and (31). We use these values to calculate growth rates by plugging the collisional and height velocities into eq. (3). The beginning and end conditions define the limits of integration for the time scale calculations.

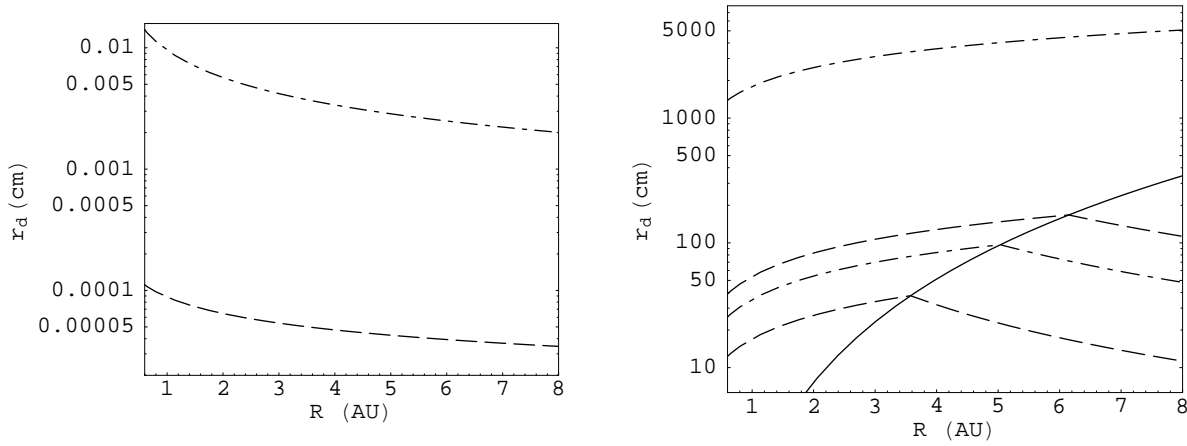


Fig. 1.1 Size of the dust grains at regime boundaries as a function of the distance from the star for $\eta = 10^{-2}$ and $\rho_d = 1 \text{ g cm}^{-3}$. The solid curve in the right plot is the dividing line between Epstein (right) and Stokes (left) drag. It lies outside the plotted region for the left plot. The lines in the left plot, from bottom to top, represent the regime boundaries between 0:1 and 1:1 and between 1:1 and 2:1 while the bottom three curves in the right plot represent the regime boundaries between 2:1 and 2:2, between 2:2 and 3:2, and between 3:2 and 3:3. The highest curve is the size at the onset of gravitational instability.

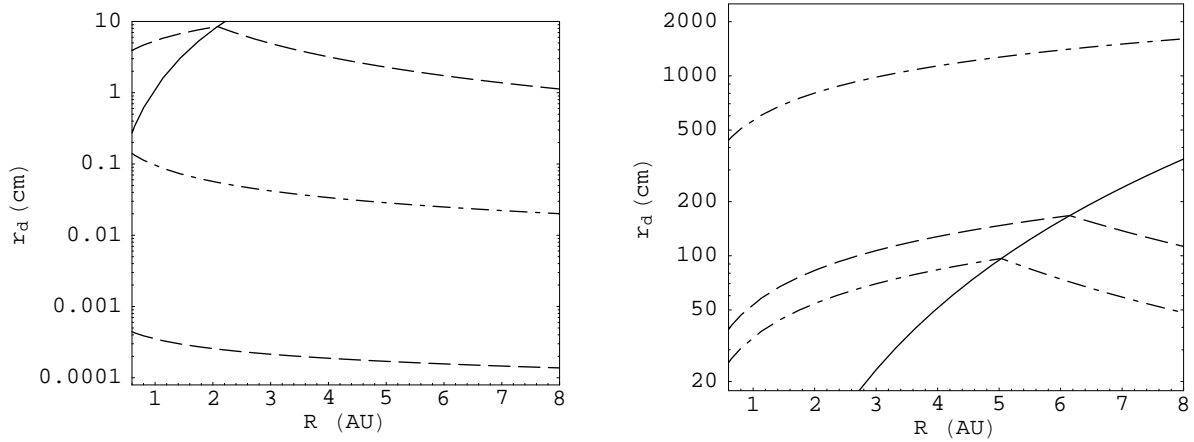


Fig. 2.1 Size of the dust grains at regime boundaries as a function of the distance from the star for $\rho = 10^{-4}$ and $\rho_d = 1 \text{ g cm}^{-3}$. The solid curve is the dividing line between Epstein (right) and Stokes (left) drag. The lines in the left plot from bottom to top, show regime boundaries between 0:1 and 1:1, between 1:1 and 2:1, and between 2:1 and 2:2 while the right plot from bottom to top, shows regime boundaries between 2:2 and 3:2 and between 3:2 and 3:3. The highest curve is the size at the onset of gravitational instability.

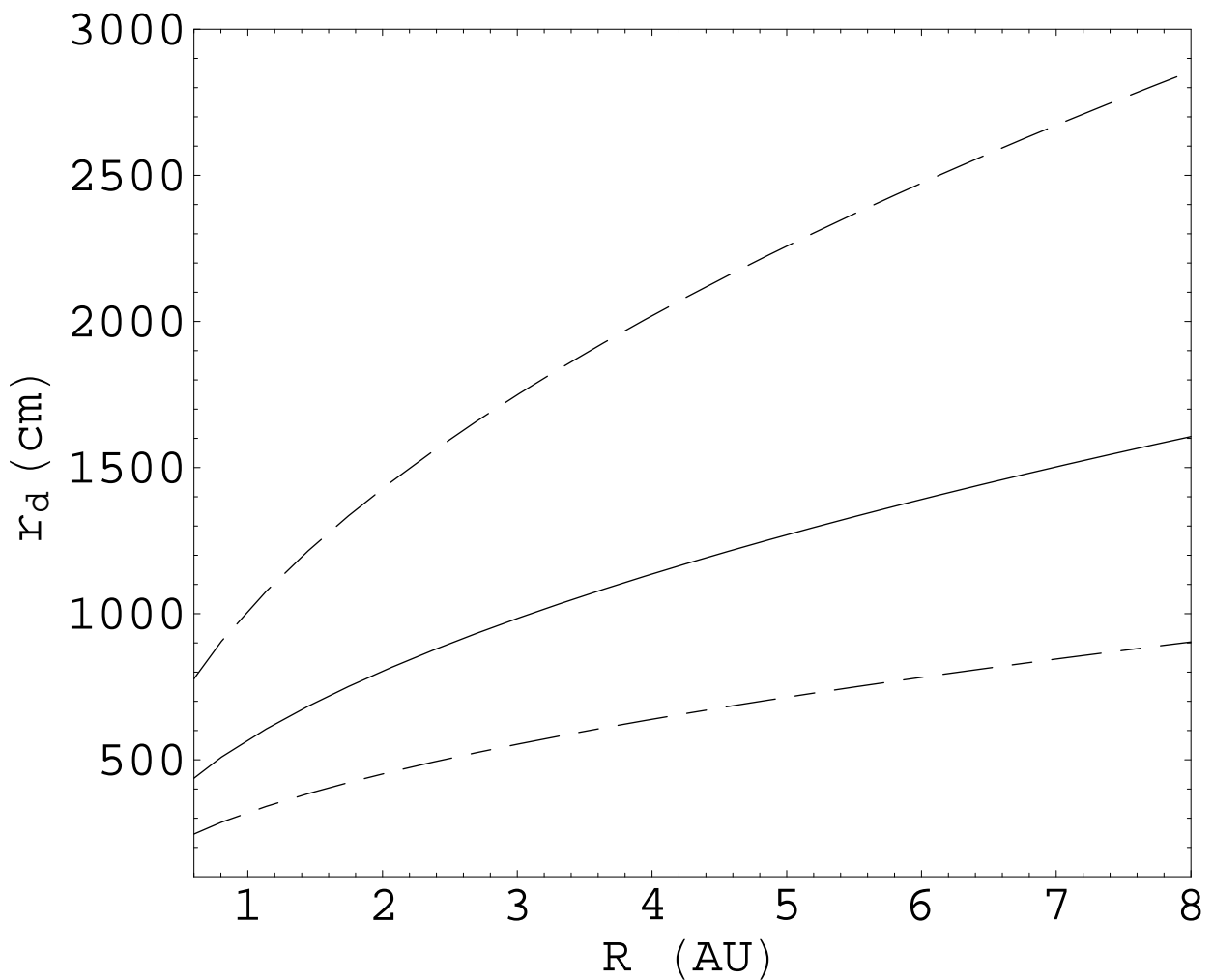


Fig. 3. The grain size at which gravitational instability occurs as a function of the distance from the star. The dashed, solid and dot-dashed lines correspond to R_d of 10^{-2} , 10^{-3} and 10^{-4} respectively.

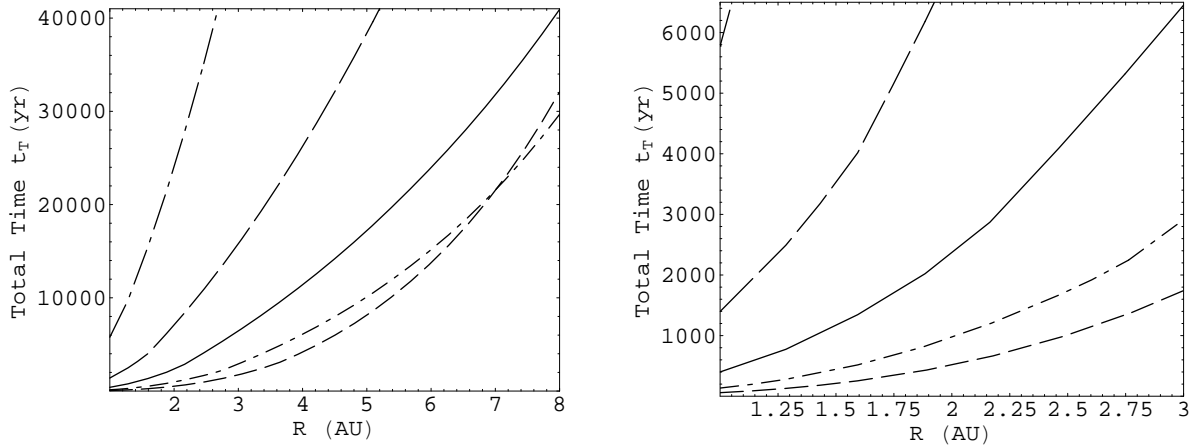


Fig. 4. Total time scales to grow through all regimes up to the gravitationally unstable regime for various values of α as a function of distance from the star. The solid line is $\alpha = 10^{-4}$. The short dashed and dot-dashed lines are α of 10^{-2} and 10^{-3} respectively while the long dashed and dot-dashed lines are for α of 10^{-5} and 10^{-6} . For any R there is a value of α that minimizes the total time scale. We have used $\rho_d = 1 \text{ g cm}^{-3}$ and $c = 1$ for these plots.

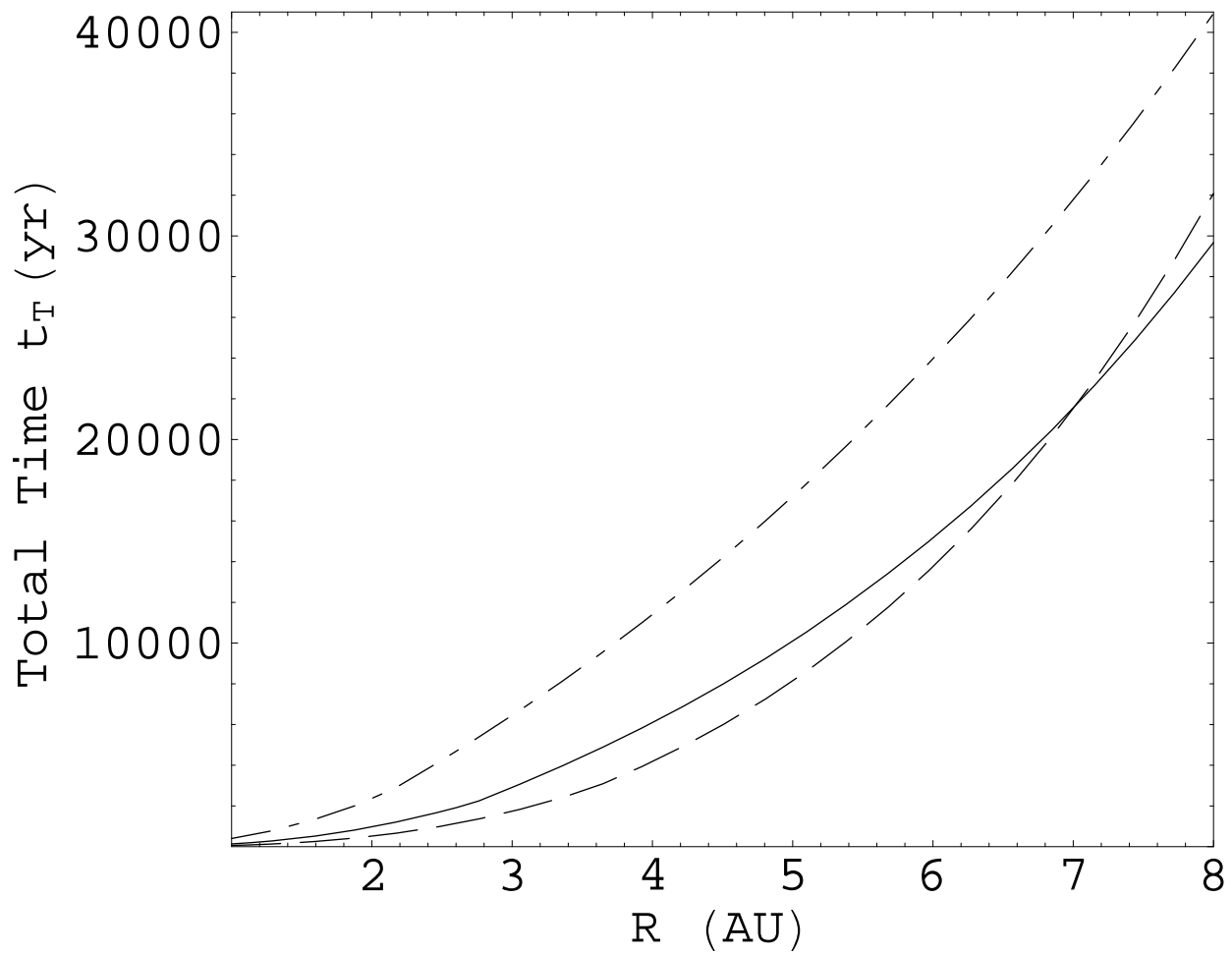


Fig. 5.1 Total growth time scales as in Fig. (4) but for a of 10^{-2} (dashed line), 10^{-3} (solid line) and 10^{-4} (dash-dotted line).

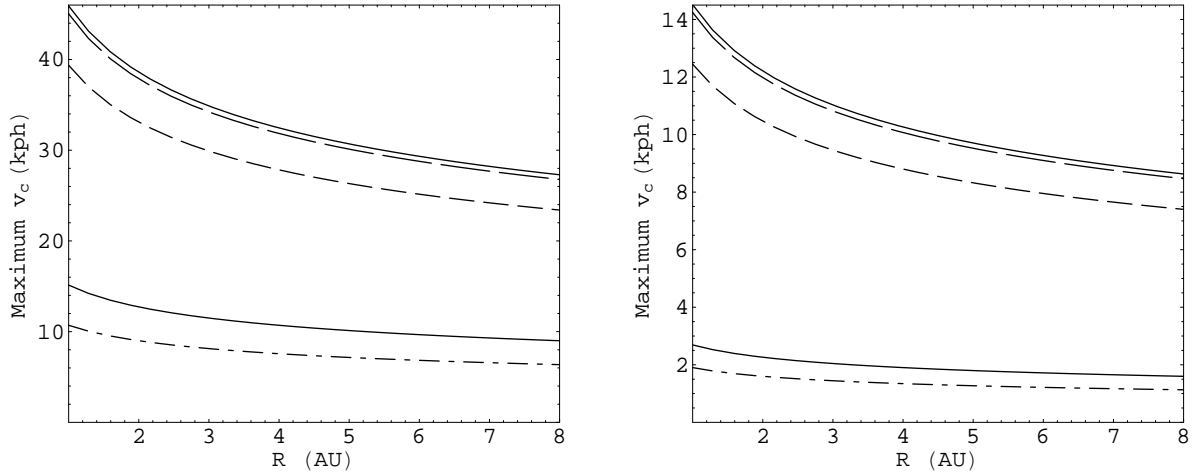


Fig. 6. Maximum collisional velocity in km/h as a function of distance from the star for a live zone of 10^3 (left) and 10^4 (right). The higher solid lines are the velocities from (28) for the live zone while the lower solid lines is the velocity from (70) for the dead zone with $H_D = 0.5H_g$ (which has 1/10 the of the corresponding live zone). The long dashed, short dashed and dash-dotted lines are the collisional velocities at the ends of regimes 3:2, 2:2 and 2:1 respectively. Because these curves apply for grains of cm to meter size scales, common experience suggests that solid grain destruction from collisions > 30 km/h would lead to obliteration rather than sticking. This renders further growth impossible for a live zone 10^3 unless there is a contemporaneous dead zone.

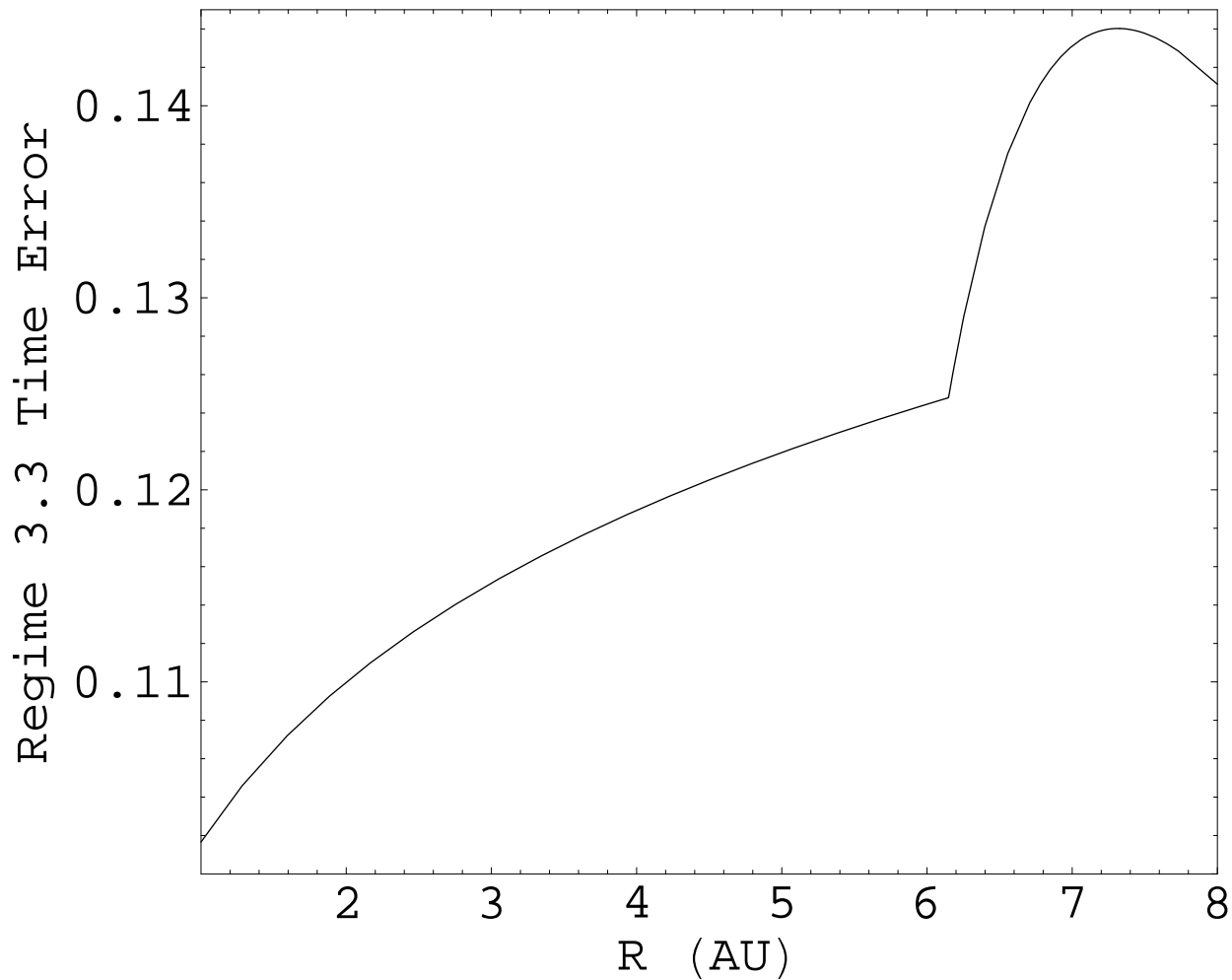


Fig. 7. | Percent error between (59) using and the numerically calculated value for the growth time in regime 3:3 for $\epsilon = 4 \times 10^{-6}$. Larger values for ϵ decrease the difference.

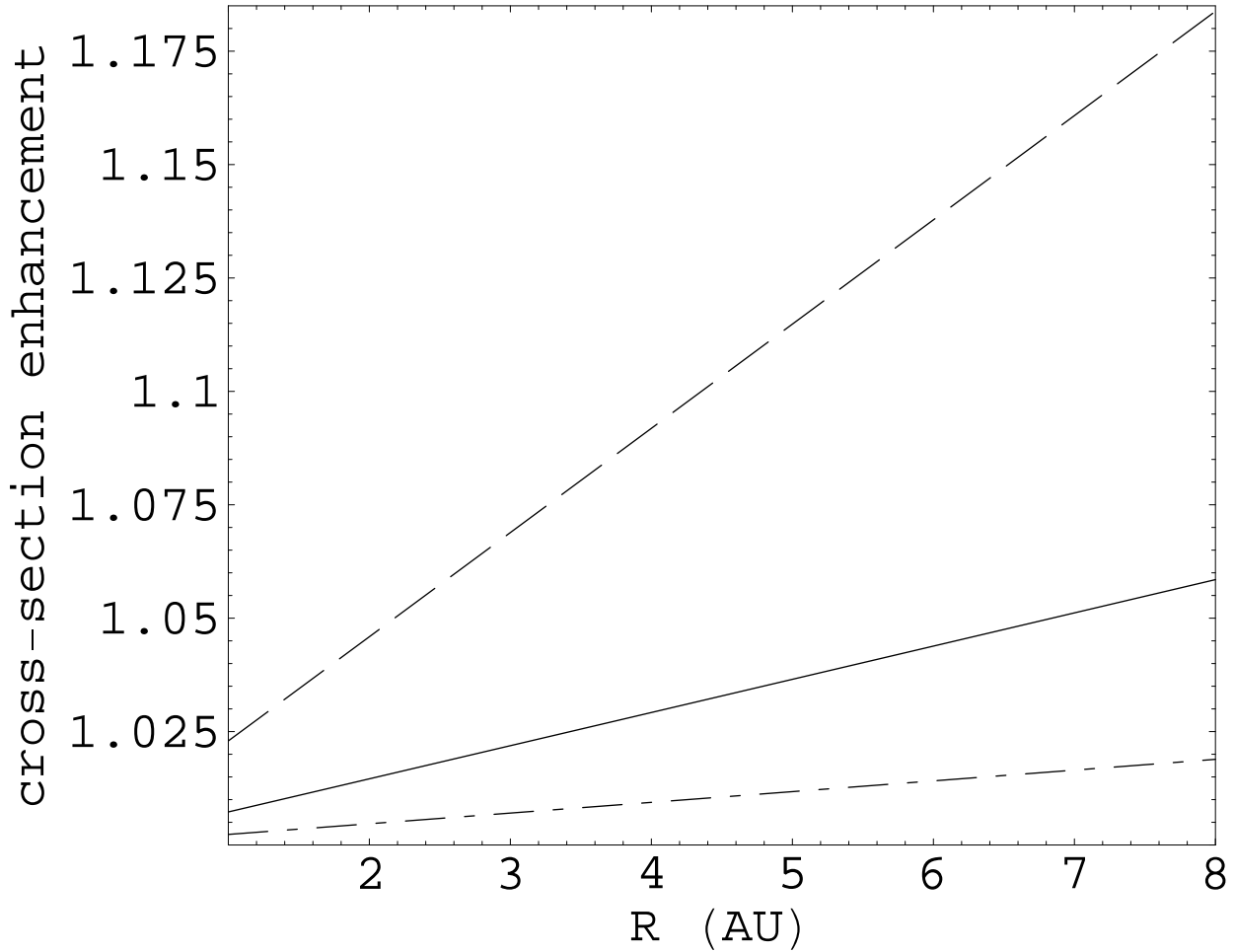


Fig. 8.1 Ratio between the gravitationally enhanced cross-section and $r_{dd} = 4 r_d^2$ at the onset of gravitational instability as a function of the distance from the star. The dashed line, solid and dash-dotted lines are of 10^{-2} , 10^{-3} and 10^{-4} respectively.

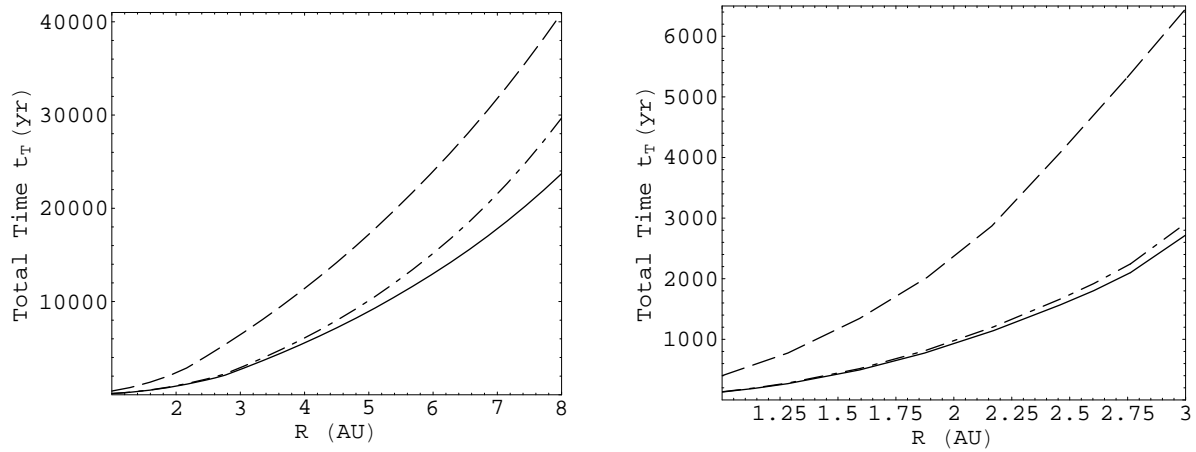


Fig. 9. The total growth time scale as in Fig. (4) but for a disc with $\alpha = 10^{-3}$ and a dead zone with $\alpha = 10^{-4}$ (solid line). Also shown are the time scales for discs of uniform $\alpha = 10^{-3}$ (dash-dotted) and $\alpha = 10^{-4}$ (dashed).

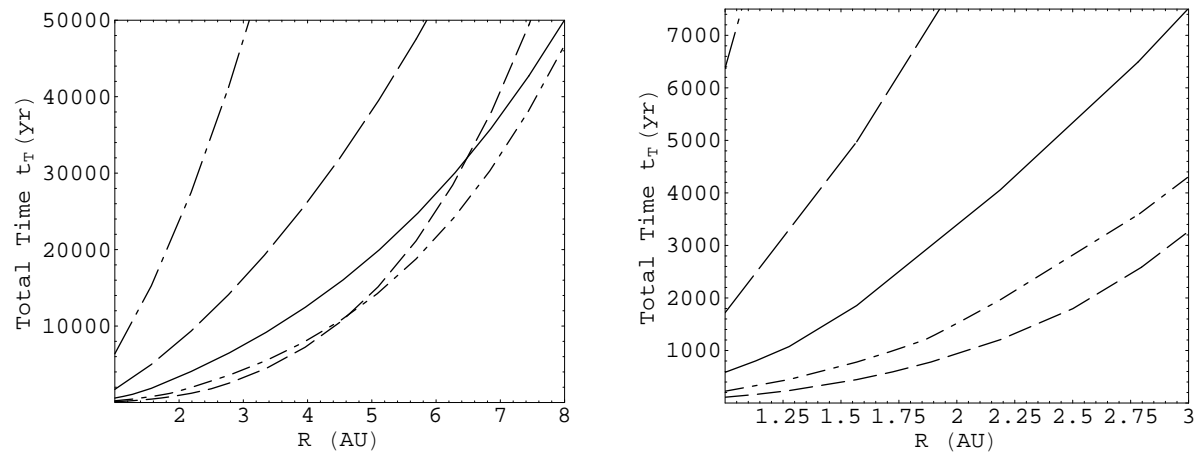


Fig. 10. Total growth time scales as a function of the distance from the star for $d = 5 \text{ cm}^3$ and $c = 1$.

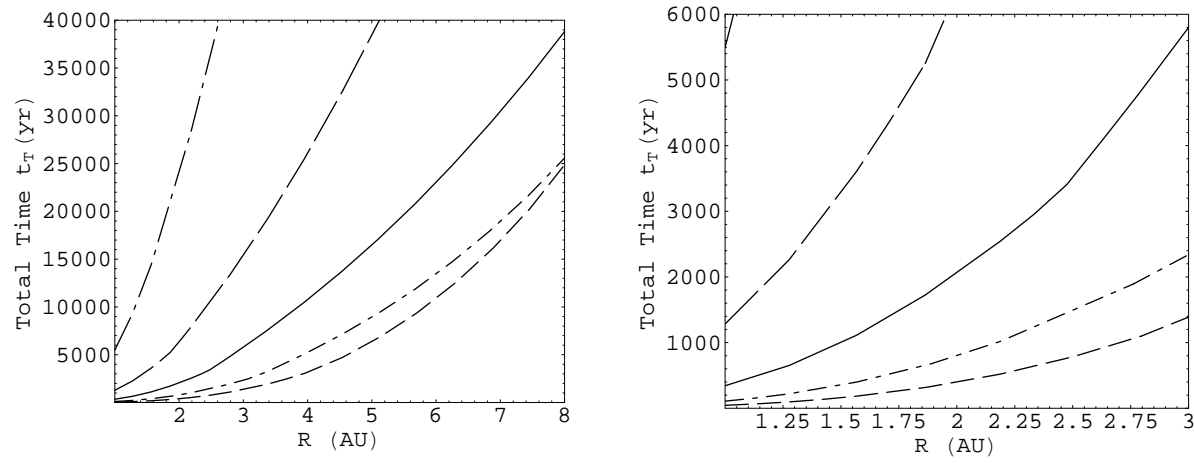


Fig. 11. Total growth time scales as a function of the distance from the star for $\rho_d = 0.5 \text{ g cm}^{-3}$ and $c = 1$.

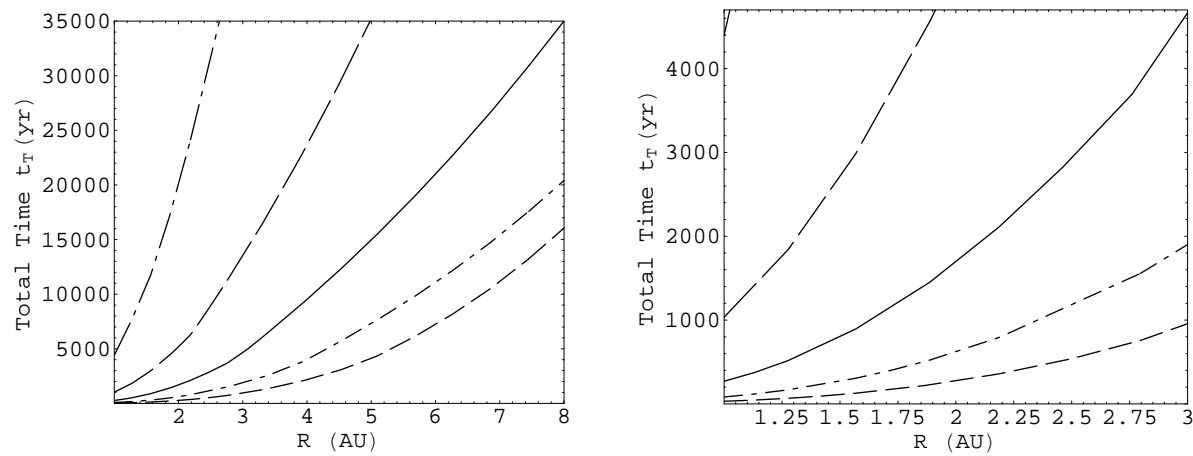


Fig. 12. | Total growth time scales as a function of the distance from the star for $g_0(1\text{AU}) = 2$, $\frac{d}{g_0} = 0.01$, $d = 1\text{cm}^{-3}$ and $c = 1$.

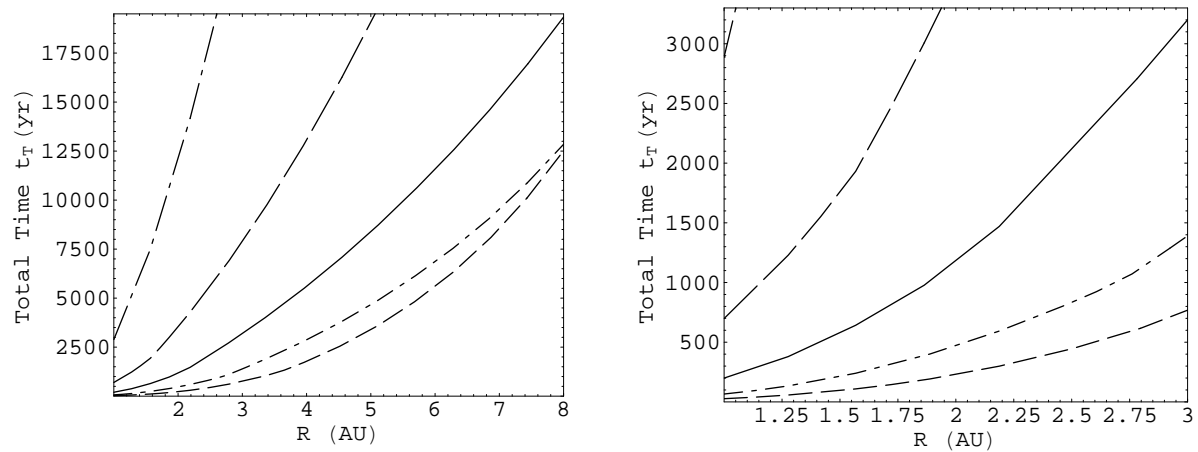


Fig. 13. | Total growth time scales as a function of the distance from the star for $g_0(1\text{AU}) = g_0, \frac{d}{g} = 0.02, d = 1\text{gcm}^{-3}$ and $c = 1$.

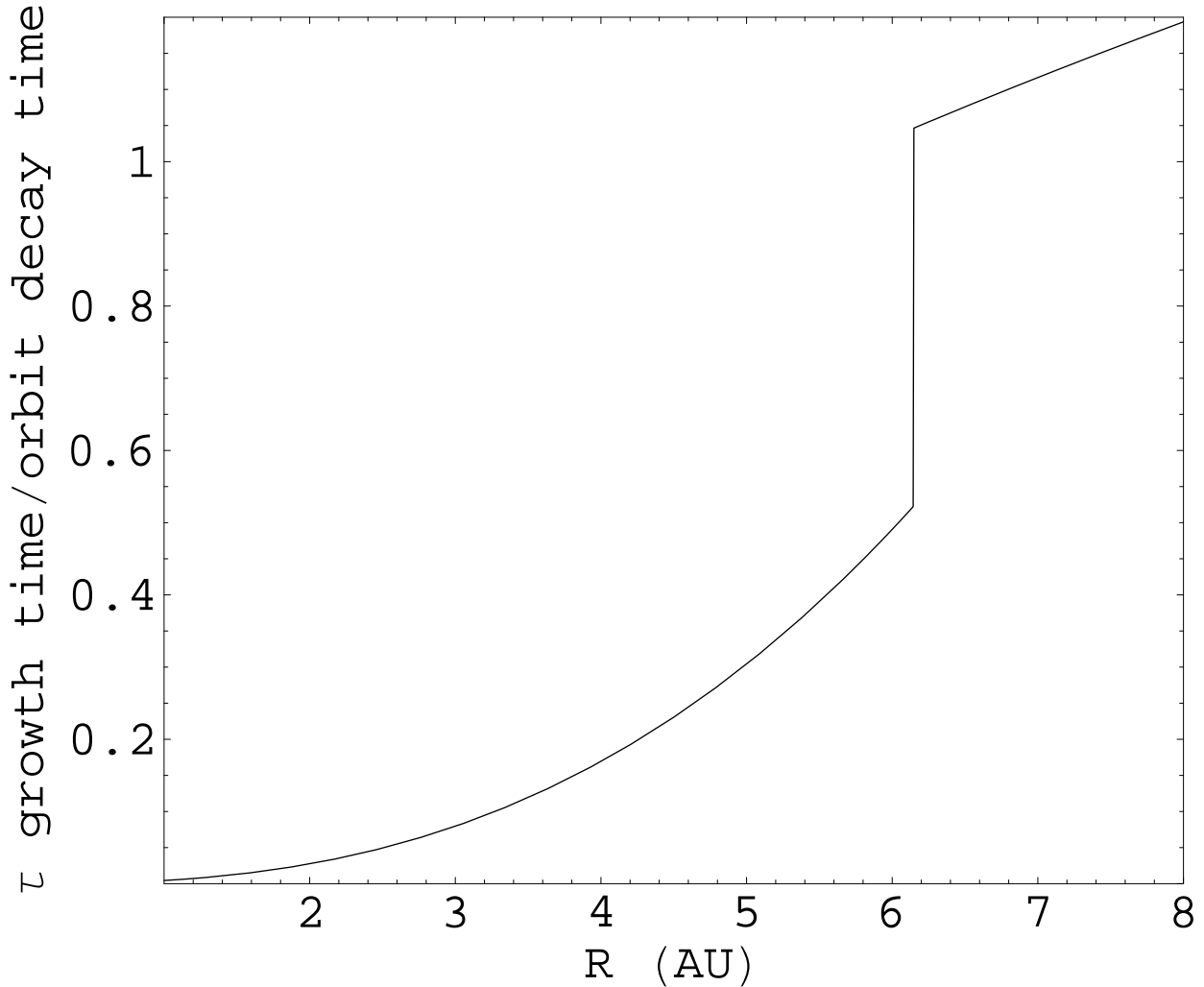


Fig. 14. The ratio of the growth time scale τ_{growth} to the infall time scale $\frac{R}{v_R}$ for the headwind induced infall as calculated in section 6.1.2, as a function of distance from the star. In this plot we take $c = 1$, but multiplying the curve by $1/c$ characterizes the result for other values of the sticking parameter. The discontinuity at $R = 6 \text{ AU}$ is due to the change in drag regime since $s = 2$ whereas $s_E = 1$.

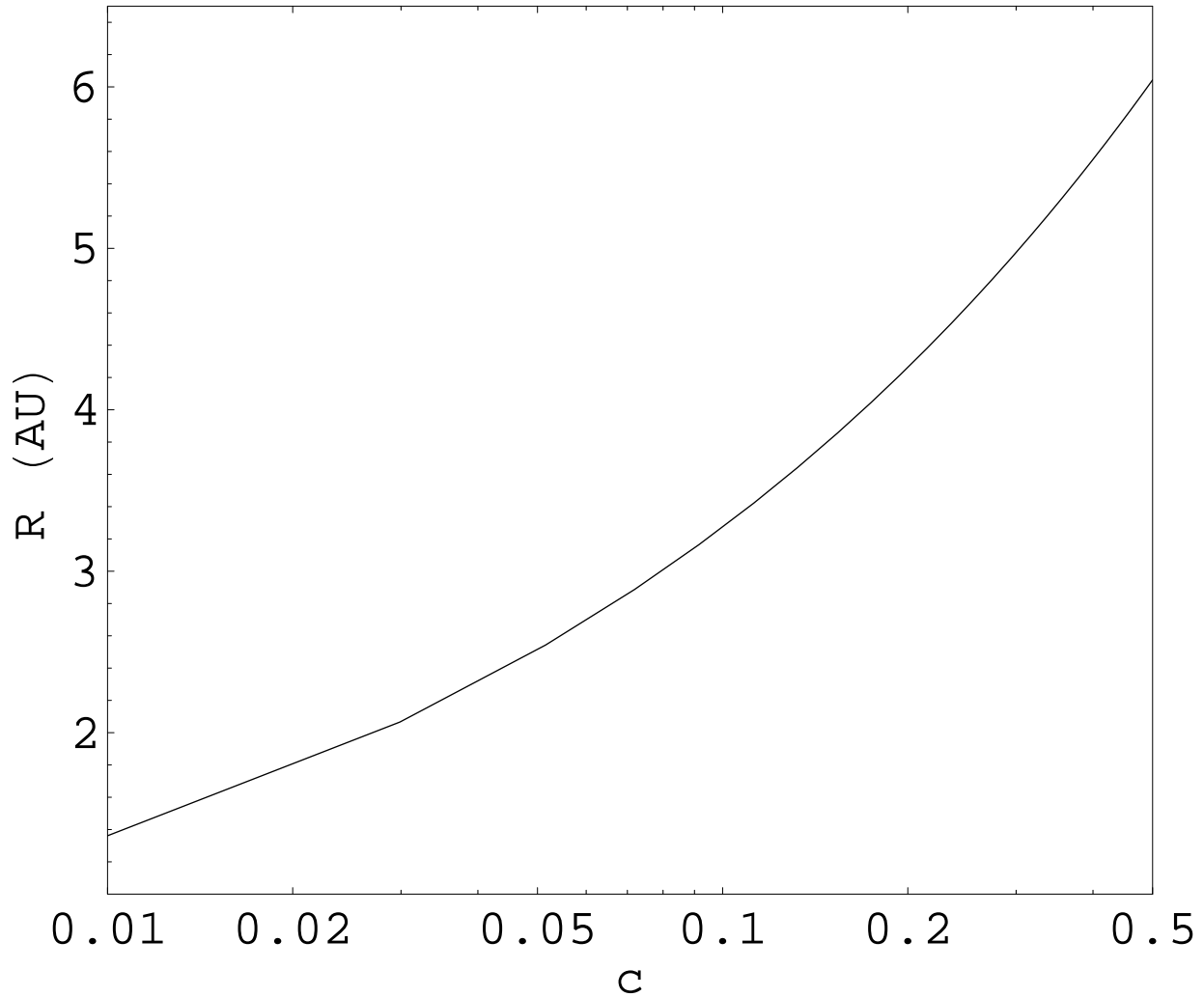


Fig. 15. The distance from the star in AU at which the headwind induced infall time of Sec. 6.1.2 equals the growth time scale of τ , as a function of the sticking parameter c . This distance is an approximate measure of the radius inside of which the headwind effect can be neglected.

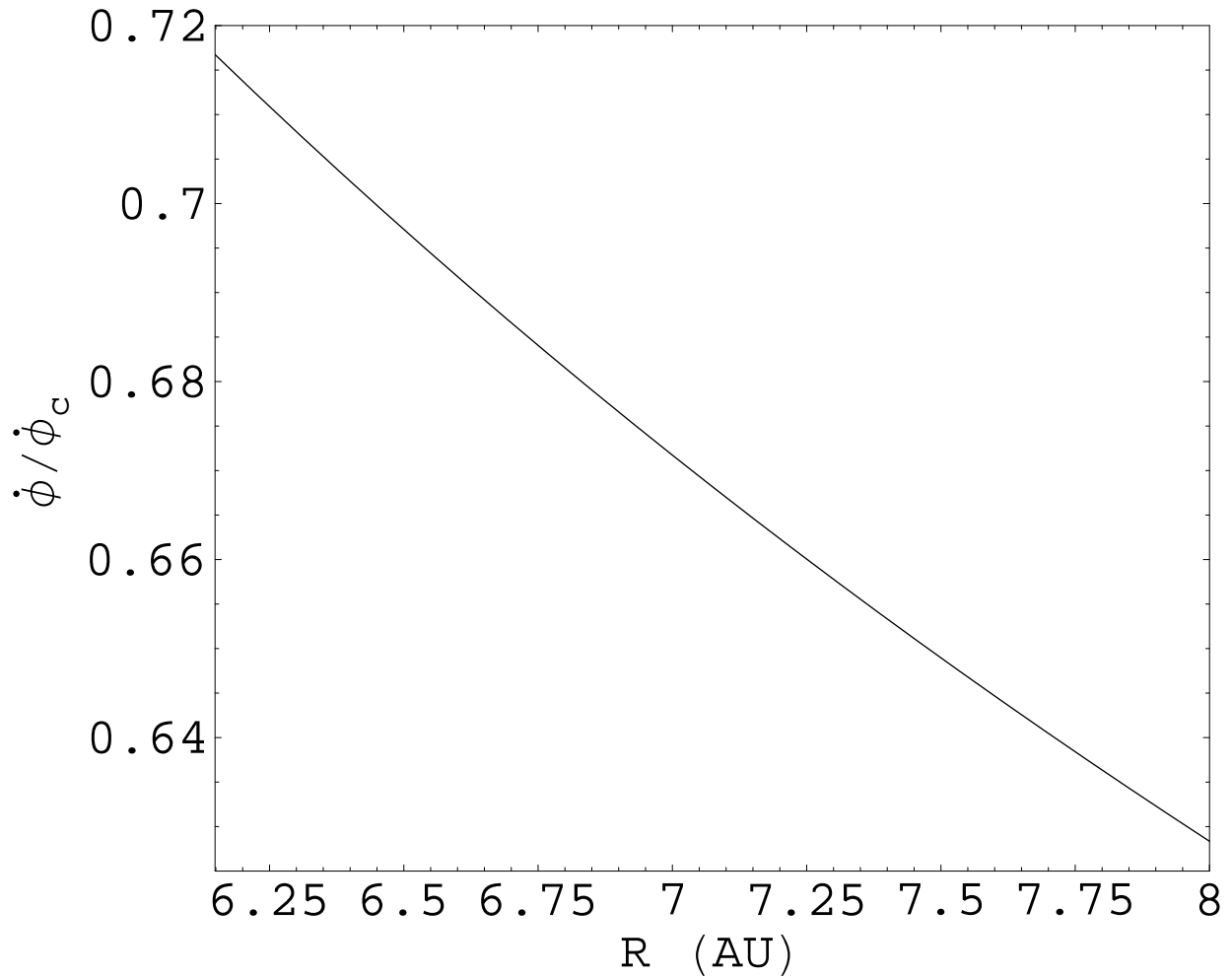


Fig. 16. | The ratio of the grain growth rate due to accretion to the growth rate of the grain size from maximum infall speed caused by the infall itself. If the ratio is less than 1 the grains cannot grow larger than that size for maximum infall speed (which for us is the boundary between regimes 3:2 and 3:3).